Novel roles of the U2 splicing complex in antiviral defence

School of Infection and Immunity
College of Medical, Veterinary & Life Sciences, University of Glasgow

Chenrui Wang, XXXXXXXX
Supervisor: Dr. Wael Kamel, Dr. Marko Noerenberg, Prof. Alfredo Castello

Acknowledgement:

I am grateful to Alfredo for giving me the opportunity to join his lab. Working in this inspiring scientific research environment strengthened my determination to continue my career in science.

I would also like to thank Wael, for his patient supervision, valuable guidance, and continuous encouragement throughout this project. His mentorship and mindset improved my scientific thinking and created an impact on my development as a researcher.

My heartfelt thanks go to Marko for his patience in teaching me the iCLIP2 technique and for patiently sharing his knowledge and experience throughout the project. His support, both scientifically and personally, was greatly appreciated.

My thanks also go to all members of the Castello lab for creating such a welcoming and supportive research environment, and to my friends for their encouragement during my time at the Centre for Virus Research.

Finally, I would like to express my deepest gratitude to my parents, Yong Wang and Yu Chen, for their love and financial support. Their support for me has made my education and scientific journey possible.

Author declaration:

I hereby declare that this thesis is the result of my own independent work conducted at the Centre for Virus Research, University of Glasgow, under the supervision of Dr. Wael Kamel, Dr. Marko Noerenberg, and Prof. Alfredo Castello. Except where otherwise indicated in the text, it is my original work.

Chenrui Wang
28th September 2025

Abstract:

Spliceosomes are essential ribonucleoprotein complexes that remove introns from nascent pre-mRNAs. Removal of introns from pre-mRNA produces mature mRNAs that are subsequently translated into proteins.

Although spliceosomes are canonically regarded as nuclear co-transcriptional complexes, emerging evidence suggests that several splicing factors also participate in cytoplasmic antiviral responses. Recent studies revealed numerous interactions between cytoplasmic viral RNAs (vRNAs) and nuclear proteins, including proteins involved in splicing.

Previous study demonstrated that specific nuclear proteins translocate to the cytoplasm during Sindbis virus (SINV) infection, which is a positive-sense RNA virus that replicates in the cytoplasm. Among those relocated proteins, the U2 snRNP complex emerged as a novel antiviral factor with activities that spanned multiple viral species and families.

Three questions motivated this study. Firstly, the triggers of the translocation of U2 snRNP and its associated proteins are unclear. Secondly, the composition of the potential antiviral complex remains unknown. It's also unclear whether U2snRNP directly binds the viral RNA or requires an adaptor complex. Finally, it remains unknown what signatures in viral RNAs the U2 snRNP recognises. This Master's project focused on clarifying the non-canonical antiviral roles of U2 snRNP cofactors and defining the viral RNA binding sites of these cofactors.

Throughout this thesis, U2AF1, U2AF2, and SF1 are collectively referred to as the U2AF complex. We hypothesised that the U2AF complex is the upstream adaptor complex facilitating the binding of U2 snRNP to SINV mRNAs.

We investigated the anti-SINV roles of the U2AF complex using loss-of-function experiments. We also optimised iCLIP2 for SF3B1, SF1, U2AF2, and AQR to establish libraries for investigating their RNA-binding profiles during SINV infection.

U2AF1 knockdown produced the strongest and most consistent increase in SINV titre, whereas SF1 knockdown showed a similar but non-significant trend and U2AF2 knockdown produced variable effects. iCLIP2 libraries were successfully generated for SF3B1, SF1, U2AF2, and AQR under infected and uninfected conditions and were suitable for sequencing.

PART 1. INTRODUCTION:

1.1 The U2AF complex in splicing

Pre-mRNA splicing is a crucial step in eukaryotic gene expression, during which introns are removed, and exons are joined to generate mature mRNA[1].
Splicing is predominantly initiated co-transcriptionally while RNA polymerase II is still transcribing the nascent pre-mRNA[2].

Splicing is catalysed by spliceosomes, which are ribonucleoprotein complexes. The major spliceosome is composed of five small nuclear ribonucleoproteins (snRNPs): U1, U2, U4, U5, and U6, together with a variety of associated pre-mRNA processing-splicing (Prp) factors[4,5,6]. During early spliceosome assembly, U1 snRNP recognises the 5′ splice site (5' ss), while factors associated with the 3′ splice-site (3' ss) region promote subsequent recruitment of U2 snRNP to the branch point[3].

The canonical U2AF heterodimer contains U2AF1 (U2AF35 and U2AF2 (U2AF65). In this thesis, U2AF1, U2AF2 and SF1 are collectively referred to as the U2AF complex. U2AF1 contributes to recognition of the conserved AG dinucleotide at the end of 3' splice site, whereas U2AF2 binds to the polypyrimidine (Py) tract. In parallel, SF1 recognises the branch point sequence. The U2AF complex, together with U1 snRNP bound at the 5′ splice site, contributes to the formation of the E complex, the earliest defined commitment complex in spliceosome assembly[3], which positions the splicing complexes for accurate recognition of introns.

Subsequent recruitment of U2 snRNP and displacement of SF1 promote the transition from the E complex to the A complex. Within the U2 snRNP, Splicing Factor 3B Subunit 1 (SF3B1) plays an important role by interacting with the branching point adenosine[10], thereby stabilising the intron in a conformation that promotes precise splicing. Subsequently, the U4, U6 and U5 tri-snRNP complex joins the spliceosome, and following the release of U1 and U4 snRNPs, the spliceosome becomes catalytically active[3]. This conformational change effectively loops the intron such that the GU site at the 5' end aligns with the AG site at the 3' end, facilitating two transesterification reactions

that excise the intron as a lariat structure.[11] (Figure 1. a)

Beyond their roles in cancer, dysregulated splicing factors are also implicated in viral infection, where pathogens hijack or are restricted by these complexes[17, 18, 19].

Figure 1. Canonical U2AF complex-mediated recruitment of U2 snRNP during pre-mRNA splicing and proposed models of U2 snRNP–viral RNA interaction.

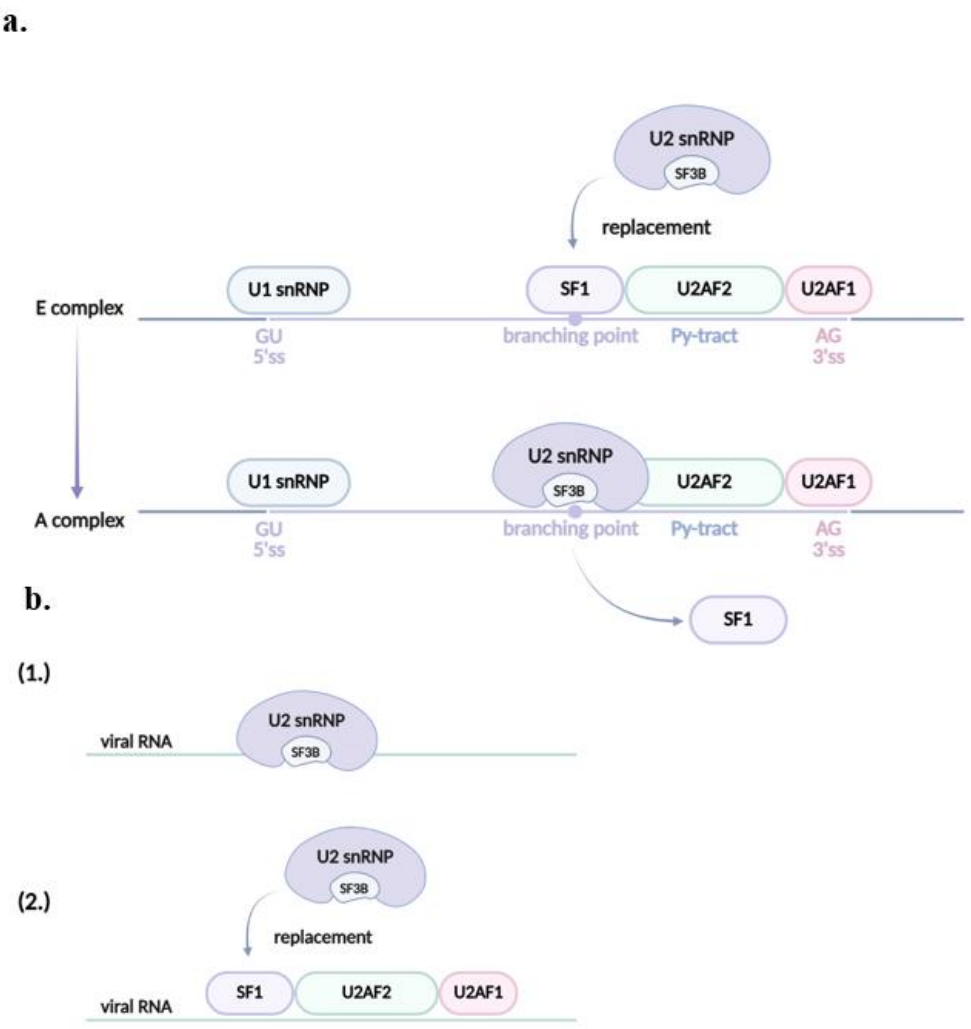

a. Schematic representation of the transition from the E to the A complex during early spliceosome assembly. U2AF1 and U2AF2 recognise the 3′ splice-site region, while SF1 binds the branch-point sequence. Recruitment of U2 snRNP to the branch-point region replaces SF1 and promotes formation of the A complex, in which SF3B1 contributes to recognition of the branch-point region. Adapted from Shao et al. (2014).

b. Two hypothesised models for the interaction between U2 snRNP and viral RNA

Direct binding model: U2 snRNP binds to viral RNA directly without requiring additional adaptor factors.

Adaptor model: The U2AF complex, defined in this thesis as U2AF1, U2AF2 and SF1, acts as an upstream adaptor that facilitates recruitment of U2 snRNP to viral RNA.

1.2 Alphaviruses

Alphaviruses represent a medically significant genus of enveloped, arthropod-borne viruses within the family Togaviridae. They possess positive-sense, single-stranded RNA genomes that can serve as direct templates for translation upon entry into host cells. Alphaviruses are broadly categorised into two groups based on geography and disease manifestation[13]: the Old World alphaviruses, such as Sindbis virus, Chikungunya virus, Ross River virus, Mayaro virus, and Barmah Forest virus, are primarily associated with febrile illness and arthralgia. In contrast, the New World alphaviruses, include Venezuelan, Eastern, and Western Equine Encephalitis viruses, are neurotropic and can cause severe encephalitis, frequently with fatal outcomes[13].

Transmission of alphaviruses predominantly occurs through mosquito vectors, enabling them to cause widespread outbreaks, particularly in tropical and subtropical regions. Despite ongoing research efforts aimed at targeting viral entry, replication, and spread, there are currently limited antiviral therapies available to combat alphavirus infections, presenting a pressing global health concern.

Alphaviruses encode five structural proteins (Capsid, E1, E2, E3, and 6K/TF) and four non-structural proteins (nsP1, nsP2, nsP3, and nsP4). Viral entry involves interactions with multiple cellular receptors and receptors[13, 14]. Following entry into host cells, alphaviruses establish bud-shaped replication organelles in the cytoplasm, which facilitate viral RNA replication. The positive-sense genomic RNA is initially translated to produce the non-structural proteins (nsPs) required for viral replication. A negative-sense RNA intermediate is subsequently synthesised and serves as a template to produce new genomic and subgenomic RNAs. The subgenomic RNA is translated to produce the structural proteins[37, 38] (Figure 2.).

Among the non-structural proteins, nsP3 is particularly relevant to virus–host interactions. It comprises three domains: a macrodomain, an alphavirus-unique domain, and a hypervariable domain. nsP3 interacts with various host proteins, including proteins that normally localise to the nucleus [14].

The SINV 3′ untranslated region (3′ UTR) contains several functionally important sequence elements[39]. A conserved sequence, together with the poly(A) tail, contributes to

the promoter required for minus-strand RNA synthesis. A U-rich sequence located upstream of this conserved region interacts with the host RNA-binding protein HuR and contributes to viral RNA stability during infection[40]. This provides an example of how specific sequence features within alphavirus RNAs can mediate interactions with host RNA-binding proteins.

While alphaviruses replicate in the cytoplasm, splicing factors canonically function in the nucleus. This spatial separation raises the question of how nuclear splicing factors encounter alphavirus RNAs and whether these interactions influence viral infection.

Figure 2. Alphavirus replication cycle and potential interactions with host splicing proteins.

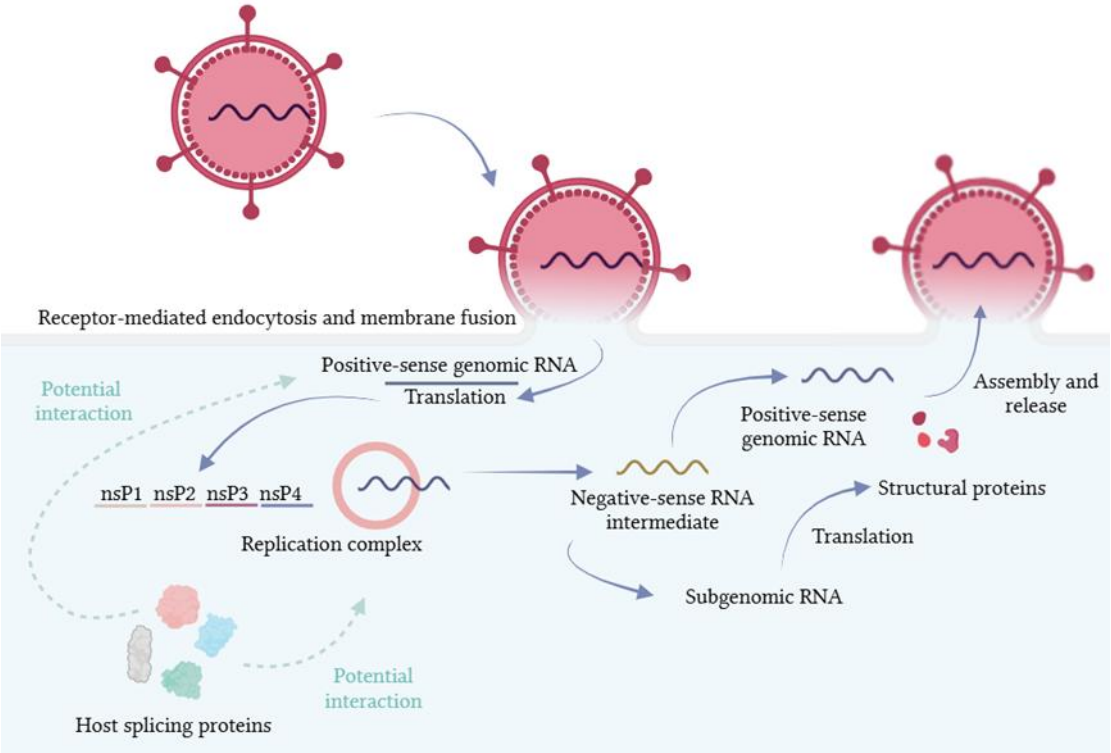

Following receptor-mediated endocytosis and membrane fusion, the positive-sense genomic RNA is released into the cytoplasm and translated to produce the non-structural proteins (nsP1–nsP4), which form the viral replication complex. A negative-sense RNA intermediate is subsequently synthesised and serves as a template for the production of genomic and subgenomic positive-sense RNAs. The subgenomic RNA is translated to produce structural proteins, which together with newly synthesised genomic RNA, contribute to the assembly and release of virions. Dashed arrows indicate potential interactions of host splicing proteins with viral RNA and the replication machinery.

1.3 Nuclear RNA-binding proteins in viral infections

Increasing evidence indicates that nuclear RNA-binding proteins can participate in virus–host interactions outside their canonical nuclear functions, with either proviral or antiviral effects[15, 16, 18].

For example, U2AF2 has been reported to translocate from the nucleus to the cytoplasm during Japanese Encephalitis Virus (JEV) infection, while depletion of U2AF2 reduced viral replication, suggesting a proviral role[18].
Conversely, the DEAD-box RNA helicase DDX39A, which also participates in pre-mRNA splicing, is reported to bind chikungunya virus (CHIKV) RNA and act as an antiviral factor[19]. Interactions between alphavirus proteins and nuclear factors are also reported; for example, SF3B3 and eRF3A interact with Semliki Forest virus (SFV) nsP3[24].

Together, these findings demonstrate that proteins involved in nuclear RNA processing can be redistributed or recruited during viral infection and can exert either proviral or antiviral effects.

1.4 Rationale and model

Kamel et al. (2024) demonstrated that SINV infection induces the cytoplasmic translocation of various nuclear RNA-binding proteins, including components of U2 snRNP[17]. They further identified U2 snRNP as an antiviral factor with activity against multiple viral species and families.
These findings suggest that components of the splicing machinery may perform non-canonical antiviral functions outside the nucleus.

However, how U2 snRNP associates with viral RNA in the cytoplasm remains unclear. It is unknown whether U2 snRNP binds viral RNA directly or is recruited through additional RNA-binding factors. We therefore propose two alternative models for the association of U2 snRNP with viral RNA.
In the direct-binding model, U2 snRNP binds viral RNA independently of additional adaptor factors (Figure 1b.1).
In the adaptor model, U2AF1, U2AF2 and SF1 act as an upstream adaptor complex that

facilitates recruitment of U2 snRNP to viral RNA (Figure 1b. 2).
These models provide a framework for investigating the molecular basis of U2 snRNP–viral RNA interactions during alphavirus infection.

Based on this rationale, this study investigated whether the U2AF complex contributes to the antiviral activity associated with U2 snRNP during SINV infection. We hypothesise that the U2AF complex acts as an upstream adaptor that facilitates the recruitment of U2 snRNP to viral RNA.
To test the antiviral roles of U2AF1, U2AF2 and SF1, loss-of-function experiments were performed. In parallel, iCLIP2 conditions were optimised for SF1, U2AF1, U2AF2, SF3B1 and AQR to establish a framework for future characterisation of their RNA-binding profiles during infection. Our findings indicate that components associated with the U2AF complex contribute to the restriction of SINV infection, supporting non-canonical antiviral roles for splicing-associated factors.

PART 2: MATERIALS AND METHODS

Buffer compositions, materials suppliers and catalogue numbers are listed in Tables 1, 2, 3, and Supplementary Table 3, unless otherwise stated in the text.

2.1 siRNA knockdown:

HEK293 Flp-In T-Rex (FITR) cells and A549 cells were maintained at 37 °C in a humidified atmosphere containing 5% CO_2 environment with Dulbecco's Modified Eagle Medium (DMEM; Gibco, 41965039) supplemented with 10% fetal bovine serum (FBS; Gibco, 10500064) and 1% penicillin- streptomycin (Sigma-Aldrich, P4458). They were seeded into 24-well plates at a density of mainly 1×10^5 cells per well approximately 20 hours before transfection.

On the following day, the culture medium was replaced with fresh DMEM supplemented with 5% FBS and 0.5% penicillin- streptomycin. Following an additional 1 h incubation, cells were transfected with small interfering RNAs (siRNAs; Table 1) at a final concentration of 50 nM, using X-tremeGENE 360 transfection reagent (Roche) according to the manufacturer's instructions[20]. Cells were maintained at 37 °C for 48 hours.

For infection, cells were inoculated with virus in serum-free DMEM for 1 hour at the multiplicity of infection (MOI) indicated for each experiment. The inoculum was then removed and replaced with DMEM containing 2.5% FBS, and cells were incubated for a further 18 hours at 37 °C with 5% CO_2.

2.2 Virus Transfection:

Baby Hamster Kidney (BHK) cells were used for the transfection of mCherry-tagged Sindbis virus, Semliki Forest virus, O'nyong'nyong virus, and Ross River virus. Cells were maintained at approximately 0.3×10^6 cells/mL. Cell counts were determined by mixing 10 µL of cell suspension with 10 µL of Trypan blue, followed by manual counting. Cells were transfected in medium adjusted to 2% FBS.

At 24 hours after seeding, 600 µL of Opti-MEM was added to microcentrifuge tubes, along with plasmid DNA, following the instructions provided by the X-tremeGENE 360

transfection reagent manufacturer. Subsequently, this transfection mixture was added to each 25 mL flask containing BHK cells. At 24 hours post-transfection, cells were examined under a fluorescence microscope to assess infection.

Virus-containing supernatants were then collected into 15 mL conical tubes, centrifuged at 2,000 rpm for 5 minutes at 4°C, and filtered through 0.45 μm filters using syringe-driven filtration. The clarified virus-containing supernatants were then aliquoted and stored at –80 °C until further analysis.

Table 1: siRNAs and optimisation conditions used for U2AF complex knockdown.

a.

Protein target:	Code:
U2AF1	AM16708-18486
	AM16708-289615
U2AF2	AM16708-19346
	AM16708-136383
SF1	AM16708-284704
	AM16708-284705

b.

trial	Reagent	Duration	Layout	Outcome	MOI
1	XTREME 360	24 hours	once	/	0.1
2~5	XTREME 360	48 hours	once	/	0.1
6	Lipofectamine	72 hours	once	/	0.1
7	Lipofectamine	48 hours	once	/	0.1
8	XTREME 360	24+24 hours	25 nM 1st day, 25nM 2nd day	/	0.1
9	XTREME 360	24+24 hours	25 nM 1st day, 50nM 2nd day	/	0.1
10	XTREME 360	48 hours	combination	Effective	1
11~13	XTREME 360	48 hours	combination	Effective	0.5

2.3 Plaque Assay:

Vero cells were seeded into 12-well plates at a density of 3×10^5 cells per well. At 24 h post-seeding, 10-fold serial dilution of the viral stock or infectious supernatant was prepared in serum-free DMEM (10^{-2} to 10^{-5} for infectious supernatants, and from 10^{-3} to 10^{-6} for viral stock).

A total volume of 500 μL of each dilution was used to infect the monolayers. Plates were incubated at 37 °C with 5% CO_2 for 1 h, with gentle rocking every 15 minutes to ensure even distribution of the inoculum.

After adsorption, 2 mL of a 0.6% Avicel overlay medium was added to each well. This overlay was prepared by mixing a 2.4% Avicel stock solution at room temperature, 1× Phosphate-buffered saline (PBS), and pre-warmed 2× MEM supplemented with 4% FBS in a 1:1:2 ratio. The plates were then incubated for an additional 48 hours at 37°C with 5% CO_2.

Following incubation, the overlay medium was aspirated. The cells were then fixed with 4% formaldehyde for 1 hour. Following fixation, the formaldehyde was aspirated and disposed of properly, and the cells were stained with a crystal violet solution for approximately 15 minutes. The stain was then rinsed off with water, and plates were allowed to air-dry before counting plaques to determine viral titres.

2.4 Pladienolide B (PlaB) treatment:

At 2 hours before infection, PlaB was prepared by diluting the 2 mM stock solution 1:1000 in serum-free DMEM to obtain a 2 μM intermediate concentration. From this, either 5 μL or 50 μL of the 2 μM PlaB solution was added per mL of serum-free DMEM with a final concentration of 10 nM, 50nM and 100 nM. Cells were then incubated with PlaB at 37 °C for 2 hours. Following this pre-treatment, the medium was removed, and the cells were inoculated with virus-containing medium at 37 °C for 1 hour to allow for infection. The inoculum was then removed and replaced with medium containing 2% FBS, and cells were incubated at 37 °C for the planned duration of each experiment.

2.5 EVOS imaging

Twenty minutes before harvesting, plates were imaged using an EVOS fluorescence microscope, and pictures were acquired using 4× and 10× lenses.

2.6 Cell lysis

Following collection of the infectious supernatant, the cell suspensions were centrifuged at 2,000 rpm for 5 minutes at 4 °C. The resulting pellets were washed once with PBS and centrifuged again under the same conditions.

Cell lysis was performed using lysis buffer 3 (50 mM HEPES, pH 7.9), 150 mM NaCl, 0.5% sodium deoxycholate, 0.1% SDS, 0.1% benzonase and 0.1mM AEBSF serine

protease inhibitor. Samples were vortexed thoroughly to resuspend the pellets and incubated at 4 °C for at least 1 hour or stored at –20 °C if needed.
Subsequently, 40 µL of 10× SDS and 40 µL of 1 M DTT were added to each tube, followed by vortexing and boiling for 5 minutes. Where insoluble debris was observed, samples were clarified by centrifugation at 16000 rpm at room temperature.

2.7 Western blot and imaging:

For Western blot analysis, 40 µL of each sample was transferred into fresh Eppendorf tubes and mixed with 10 µL of 4 × LDS/2 × Laemmli sample buffer. Samples were loaded onto BioRad Precast gel, and electrophoresis was performed using SDS running buffer (diluted 1:9 in Milli-Q H_2O) at 180 V for 40 minutes. Proteins were transferred to bioRad nitrocellulose membrane. Transfer programmes were selected based on the molecular weights of the target proteins.
Membranes were blocked in milk-PBS solution on a vortex platform for 30 minutes to 1 hour, then incubated overnight at 4°C with primary antibodies (Table 2). Following incubation, membranes were washed at least twice with 0.04% PBS-Tween solution for 10 minutes each wash.
Subsequently, membranes were incubated with secondary antibodies in blocking buffer at a concentration of 0.01% and were washed 3 times and then imaged by the LICOR Odyssey CLx machine.

2.8 Immunoprecipitation and silver staining

HEK293 Flp-In T-Rex cells were seeded at a concentration of 3×10^7 cells per flask 24 h before harvesting. On the day of harvest, cells were rinsed with 10 mL of PBS and detached using a cell scraper. The cell suspension was collected and centrifuged at 200 × g. The cell pellet was then resuspended in PBS and transferred to a 15 cm Petri dish for UV crosslinking at 254 nm with an energy setting of 150 mJ. Following crosslinking, cells were collected again, centrifuged at 200 × g.
Subsequently, approximately 6×10^7 cells were lysed in 2 mL of iCLIP2 lysis buffer and incubated on ice for 30 minutes. The lysate was then centrifuged at 4°C at 16100 rpm. To each sample, 4 U of Turbo DNase (AM2238) and 1 µL of AEBSF protease inhibitor were added. 100 µL of the resulting lysate was removed and set aside as the input control.

Subsequently, 200 µL of the lysate was incubated with 0.5 µg of the specific antibody for 1 hour on a rotator at 4 °C. Following this, 10 µL each of magnetic Protein A beads and Protein G were added, and the samples were incubated for an additional hour under the same conditions.

After incubation, the samples were subjected to six sequential washes with washing buffers: 2 times with iCLIP2 high salt buffer. 2 times with medium salt buffer, and finally 2 times with PNK washing buffer.

After removal of the supernatant, the samples were resuspended in 50 µL of 1 ×LDS sample buffer (comprising 12.5 µL of 4 × LDS, 0.5 µL of 1 M DTT, and 37 µL of PNK washing buffer) and heated at 95°C for 5 minutes. The samples were loaded onto BioRad precast gels for Western blot and silver staining.

Silver staining was performed using a protocol adapted from the SilverQuest™ Silver Staining Kit manual.[22]

Table 2. Primary antibodies used:

Target protein	Molecular weight (kDa)	Cat no.	Type
SF3B1	155	27684-1-AP	Rabbit Polyclonal
SF3B1	155	HPA050275	Rabbit Polyclonal
AQR	171	24342-1-AP	Rabbit Polyclonal
AQR	171	HPA055647	Rabbit Polyclonal
U2AF1	35	60289-1-Ig	Mouse monoclonal
SF1	68	ab223256	Rabbit Recombinant Monoclonal
U2AF2	65	U4758	Mouse monoclonal
Beta-Actin	42	AB_476692	Mouse monoclonal
SINV Capsid	34	Laboratory of L. Carrasco	Rabbit polyclonal
mCherry	100/30	AB_2876881	Rabbit Polyclonal
p-SF3B1	>155	AB_2798893	Rabbit monoclonal

2.9 Individual-nucleotide resolution crosslinking and immunoprecipitation version 2 (iCLIP2) (Figure 3.)

This protocol was adapted by Dr. Marko Noerenberg, from the original protocol described by Buchbender et al. (2020)[32].

Figure 3. Schematic overview of the iCLIP2 workflow used in this study.

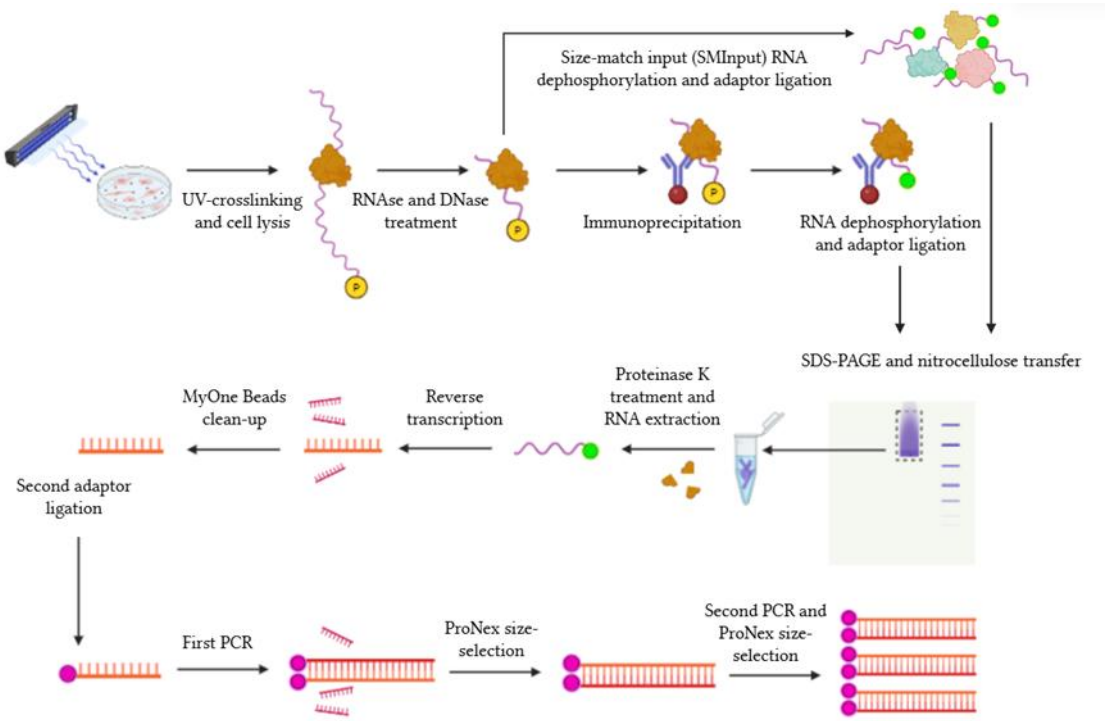

Protein–RNA interactions were stabilised by UV crosslinking, followed by cell lysis and RNase and DNase treatment. A fraction of the lysate was retained as the size-matched input (SMI) control, while the remaining lysate was subjected to immunoprecipitation to isolate the protein of interest and associated RNA fragments. Immunoprecipitated RNA was dephosphorylated and ligated to the L3-IR-App adaptor. SMI samples were processed separately for RNA dephosphorylation and adaptor ligation. Both immunoprecipitated and SMI samples were subsequently subjected to SDS–PAGE and transferred to a nitrocellulose membrane. Following proteinase K treatment and RNA extraction, RNA fragments were reverse transcribed into cDNA. The cDNA was purified using MyONE beads, ligated to the second adaptor, amplified by PCR and subjected to ProNex size selection to generate the final iCLIP2 libraries.

Table 3. iCLIP2 buffer composition

iCLIP2 high-salt buffer	1 M NaCl, 50 mM Tris-HCl, pH 7.5, 1 mM EDTA, 1% NP-40, 0.1% SDS and 0.5% sodium deoxycholate
medium-salt buffer	250 mM NaCl, 20 mM Tris-HCl, pH 7.5, 1 mM $MgCl_2$, 0.05% NP-40
PNK washing buffer	20 mM Tris-HCl, pH 7.5, 10 mM $MgCl_2$ and 0.2% Tween-20
5X PNK buffer, pH 6.5	350 mM Tris-HCl, pH 6.5, 50 mM MgCl2, 5 mM Dithiothreitol
Proteinase K buffer	100 mM Tris-HCl, pH 7.4, 50 mM NaCl, 10 mM EDTA, 0.1% SDS

2.9.1 Lysate generation

HEK293 Flp-In T-REx cells were seeded at a density of 3×10^7 cells per T150 flask 20 hours prior to infection. Cell numbers were counted at seeding and doubled to estimate the number present at the time of infection.
Cells were infected with SINV-WT at a multiplicity of infection (MOI) of 2 in serum-free DMEM. At 1 h after infection, the medium was replaced with DMEM supplemented with 2% FBS, and cells were harvested 18 hours after the medium change. Uninfected control samples were harvested at the same time point. The samples were subjected to UV crosslinking at doses of either 150 mJ or 300 mJ for optimisation, whereas 600 mJ was used for the final experiment. Cells were then lysed as described in Section 2.8.

2.9.2 Immunoprecipitation

TURBO DNase was added to the samples at a concentration of 4 units (2 µL) per sample and mixed thoroughly by vortexing. Ambion RNase was diluted in ice-cold PBS to the concentrations specified for each experimental condition. Following vortex mixing, samples were incubated at 37 °C with shaking at 1,100 rpm for 3 minutes and then placed on ice for at least 3 minutes. RiboLock RNase inhibitor (40 U/µL) was then added at 5 µL (200 units) per mL of sample. Two 10 µL aliquots (1.25% and 0.5% corresponding to the immunoprecipitation samples) were collected as size-matched input (SMInput) controls and stored at –80 °C.
Immunoprecipitation was performed by adding 2 µg of appropriate antibody to each lysate treated with RNase, followed by incubation for 1 hour at 4 °C with rotation. Pre-washed Dynabeads™ Protein A for Immunoprecipitation (ThermoFisher, 10002D) and Dynabeads™ Protein G for Immunoprecipitation (ThermoFisher, 10009D) were then added to the samples. Samples were rotated for an additional hour at 4 °C.
Beads were separated on a magnetic rack and washed sequentially twice with 1 mL of high-salt buffer, twice with 1 mL of medium-salt buffer and twice with 1 mL of PNK washing buffer (Table 3.).

2.9.3 Dephosphorylation and adaptor ligation

The 3'-end dephosphorylation mixture was prepared by combining 14.5 µL H_2O, 4 µL 5× PNK buffer pH 6.5, 5 U (0.5 µL) T4 Polynucleotide Kinase (M0201L), 0.25 U (0.25 µL) FastAP alkaline phosphatase (EF0654), 0.5 U (0.25 µL) TURBO DNase, and 20 U (0.5 µL) RiboLock RNase inhibitor with each sample. Then, samples were incubated for 40 minutes at 37˚C, shaking at 1,100 rpm, followed by washing once with PNK washing buffer, twice with high-salt buffer and once with PNK washing buffer. The L3-IR-App adaptor ligation mixture was adapted from Zarnegar et al. (2016)[34] was prepared by mixing 3.6 µL H_2O, 2 µL 10× T4 ligation buffer (with 1 mM DTT; ThermoFisher EL0021), 10 U (1 µL) T4 RNA ligase I high concentration (M0437M), 20 U (0.5 µL) Ribolock RNase inhibitor, 4 U (0.4 µL) T4 Polynucleotide Kinase (M0201L), 2.5 µL diluted L3-IR-App adaptor (1:10 dilution of 1 µM stock; final ~16.66 nM), 9 µL (40%) PEG8000 (MERCK, P1458), and 1 µL 100% DMSO (ThermoFisher, D12345). Samples were incubated at 16˚C overnight, with shaking at 1,100 rpm. Samples were washed once with PNK washing buffer, twice with high-salt buffer and once with PNK washing buffer.

2.9.4 SDS-PAGE

The SDS-PAGE-LDS buffer was prepared with 5 µL 4 × NuPAGE sample buffer, 2 µL 1 M DTT (final 10%), and 13 µL PNK washing buffer. For size-matching input (SMI) samples, 5 µL 4 × NuPAGE sample buffer, 2 µL 1 M DTT, and 3 µL PNK washing buffer were mixed with 10 µL of cell lysates. Samples were heated at 70 °C for 5 minutes and then centrifuged at 2,500 rpm for 2 minutes and then loaded on 4-20% BioRad Precast gels. Electrophoresis was performed at 180 V for 45 minutes, and the proteins were transferred to an iBlot nitrocellulose membrane using the BioRad Trans-Blot Turbo programme: 10 minutes, 25 V, 1.25 A.

2.9.5 RNA extraction

The membrane was transferred to 350 µL proteinase K buffer. 20 µL (400 µg) of recombinant, PCR-grade Proteinase K (MERCK, 3115836001) was added to each sample and incubated for 1 hour at 50 °C and 1,100 rpm. The supernatant was

transferred to a new Eppendorf tube, and the membrane pieces were rinsed with 50 µL proteinase K buffer. 400 µL of Phenol: Chloroform: Isoamyl Alcohol (pH 6.6-6.9) was mixed with each sample and incubated for 10 minutes at 37 °C and 1,100 rpm. RNA was extracted using the Zymo-Spin IC kit[23] and eluted in nuclease-free water.

2.9.6 Size-matching input (SMI)

Following RNA extraction, 4.5 µL H_2O, 4 µL 5× PNK buffer pH 6.5 (T2194-1L), 5 U (0.5 µL) PNK enzyme (M0201L), 0.5 U (0.5 µL) FastAP alkaline phosphatase (EF0654), and 20 U (0.5 µL) RiboLock RNase inhibitor were added with the RNA eluate. Samples were incubated for 40 minutes at 37˚C,1100 rpm.
For purification, 60 µL of MyONE magnetic beads, 2 µL of 5 M NaCl, and 123 µL of 100% Ethanol were added to each sample. The beads were subsequently washed three times with 80% ethanol. The samples were eluted in 5 µL nuclease-free water
The eluates were ligated with 0.7 µL H_2O, 2 µL 4× T4 ligation buffer (Thermo EL0021), 15 U (1.5 µL) T4 RNA ligase I high concentration (EL0021), 20 U (0.5 µL) RNase inhibitor (RiboLock), 2 µL diluted L3-IR-App adaptor (1:10 dilution of 1 µM stock), 8 µL PEG8000 (40%), and 0.3 µL 100% DMSO. Samples were then purified using MyONE magnetic beads
Following purification, samples were incubated for 1 hour at 37 ˚C, 1,100 rpm with 2.5 µL H_2O, 2 µL NEB Buffer 2, 25 U (0.5 µL) 5′ Deadenylase (M0331S), 15 U (0.5 µL) RecJf exonuclease (M0264S), 20 U (0.5 µL) RiboLock RNase inhibitor, and 4 µL PEG8000 (40%). Samples were subsequently purified by MyONE magnetic beads as described above.

2.9.7 Reverse transcription, adaptor ligation and DNA purification

1 µL of 0.5 µM RT oligo and 1 µL of 10 mM dNTP mix were added to each sample. Samples were incubated at 70 °C for 5 min. Samples were then supplemented with 2 µL of H_2O, 4 µL of 5× SSIV buffer, 1 µL of 0.1 M DTT, 20 U (0.5 µL) of RNase inhibitor, and 100 U (0.5 µL) of SuperScript IV enzyme (ThermoFisher, 18090010), and incubated according to the RT programme. Then, 2.5 µL of 1 M NaOH was added to each sample, followed by incubation at 85°C for 15 minutes. Samples were then neutralised by adding 1 M HCl.

cDNA was purified using MyOne silane beads. 10 µL of beads were resuspended in 78 µL of RLT per sample with an addition of 93.6 µL 100% ethanol. Samples were incubated for 10 minutes, then washed three times with 900 µL of 80% ethanol and air-dried for 5 minutes at room temperature. Finally, the cDNA was eluted in 5 µL of H_2O by incubating for 5 minutes at room temperature.
Oligo adaptor (2 µL) and DMSO (1 µL) were added to each sample. Samples were then heated at 75°C for 2 minutes and immediately placed on ice. A ligation mix was prepared on ice for each sample, consisting of 0.5 µL H_2O, 3 µL T4 RNA ligase buffer, 9 µL 40% PEG8000, and 15 U (1.5 µL) T4 RNA ligase (final volume, 14 µL, including the cDNA solution). Subsequently, 12 µL of this ligation mix was added to each sample and mixed thoroughly. Samples were then incubated overnight at room temperature with shaking at 1100 rpm, followed by purification using MyOne beads as described above. PCR amplification was performed by combining 2.5 µL Solexa_s primer mix and 25 µL 2× Phusion HF Master Mix. 3 × ProNex beads were used for size selection, and then the product was eluted in 21 µL H_2O.

2.9.8 qPCR and PCR amplification

1 µL aliquot from each sample was diluted 1:10, and 1 µL of each diluted sample was combined with 3 µL H_2O, 0.5 µL 20× EvaGreen, 0.5 µL Solexa_s primer mix, and 5 µL 2× Phusion HF Master Mix. qPCR was performed according to the programme listed in the supplementary data. The cycle number at which the amplification signal reached its maximum was used for subsequent PCR amplification. PCR products were then purified using 3X ProNex selection beads for DNA cleaning, and then the samples were eluted in 25 µL H_2O. The cleanup was repeated using ProNex beads at three times the sample volume, followed by a final elution in 25 µL of H_2O.

2.9.9 TapeStation analysis and reverse size selection

The concentration of each sample was measured using a Qubit dsDNA quantitation, High Sensitivity assay. Library size distribution was measured using the High Sensitivity D5000 TapeStation. For libraries containing an excess of large DNA (>70%), a reverse size selection was performed using a protocol developed by the CVR Genomics group.

The sample volume was increased to 50 µL by adding 10 mM Tris-Cl, pH 8. 30 µL (0.6X) of AMPure reagent was then mixed with the samples at room temperature and incubated for 10 minutes. The supernatant was separated after being placed on the magnetic rack for 5 minutes. AMPure XP reagent was added to the supernatant at a final ratio of 1.8:1 and incubated for 10 minutes at room temperature. The beads were separated and washed twice with 200 µL of 80% ethanol, then air-dried for 5 minutes. DNA was eluted in 20 µL of 10 mM Tris-Cl, pH 8.0. Library size distribution was then reassessed using a High Sensitivity D5000 TapeStation.

2.10. Statistics

Data were analysed using GraphPad Prism version 10.1.2. and R version 4.5.3. For comparisons across multiple plaque assay experiments, data were normalised by calculating the ratio of each value to the corresponding control group. Statistical significance was assessed using a two-tailed unpaired t-test with Welch's correction. A significance threshold of $P < 0.05$ was used.

PART 3. RESULTS.

3.1.1 Optimisation of siRNA-mediated knockdown

To establish an experimental model for investigating the antiviral effects of the U2AF complex during alphavirus infection, four alphaviruses, SINV, SFV, ONNV and RRV, were initially evaluated. These viruses were selected to provide a panel of alphaviruses for comparison and to identify a suitable viral model for subsequent knockdown experiments. Viral stocks were therefore generated in BHK cells, and their titres were determined by plaque assay in Vero cells before proceeding with the loss-of-function experiments.

SINV exhibited a titre at approximately 1×10^7 PFU/mL followed by SFV at approximately 6×10^6 PFU/mL, and RRV at roughly 4×10^6 PFU/mL. ONNV exhibited a lower titre of approximately 2×10^5 PFU/mL after an additional 20 h. (Figure 4.) Among these viruses, SINV produced the highest titre and was selected as the primary model for subsequent knockdown experiments. SINV was also particularly relevant to this project because previous work by Kamel et al. had identified interactions between spliceosomal proteins and SINV RNA, providing a basis for investigating whether upstream U2AF complex components also contribute to antiviral restriction.

To determine whether components of the U2AF complex contribute to the restriction of SINV replication, U2AF1, U2AF2 and SF1 were depleted using siRNA-mediated knockdown. 2 siRNAs targeting each protein were initially tested in HEK293 FITR cells. A 24-hour knockdown period was initially tested (Table 1b, trial 1; Figure 5), but it did not result in sufficient reduction of the targeted proteins.
The knockdown period was therefore extended to 48 hours (Table 1b, trials 2 to 5). Under these conditions, increased viral capsid expression and mCherry fluorescence were observed following knockdown, although depletion of the target protein remained insufficient.

Alternative transfection conditions were therefore evaluated. Lipofectamine was subsequently tested as an alternative transfection reagent. A 72 h knockdown was initially performed (Table 1b, trial 6); the cells became over-confluent, preventing

reliable assessment by fluorescence microscopy. The experiment was repeated with a 48-hour knockdown period using Lipofectamine (Table 1b, trial 7). Under these conditions, no clear differences in target protein or viral capsid levels were detected by Western blot.

Figure 4: Plaque Assay quantification of SINV, SFV, ONNV and RRV viral stocks

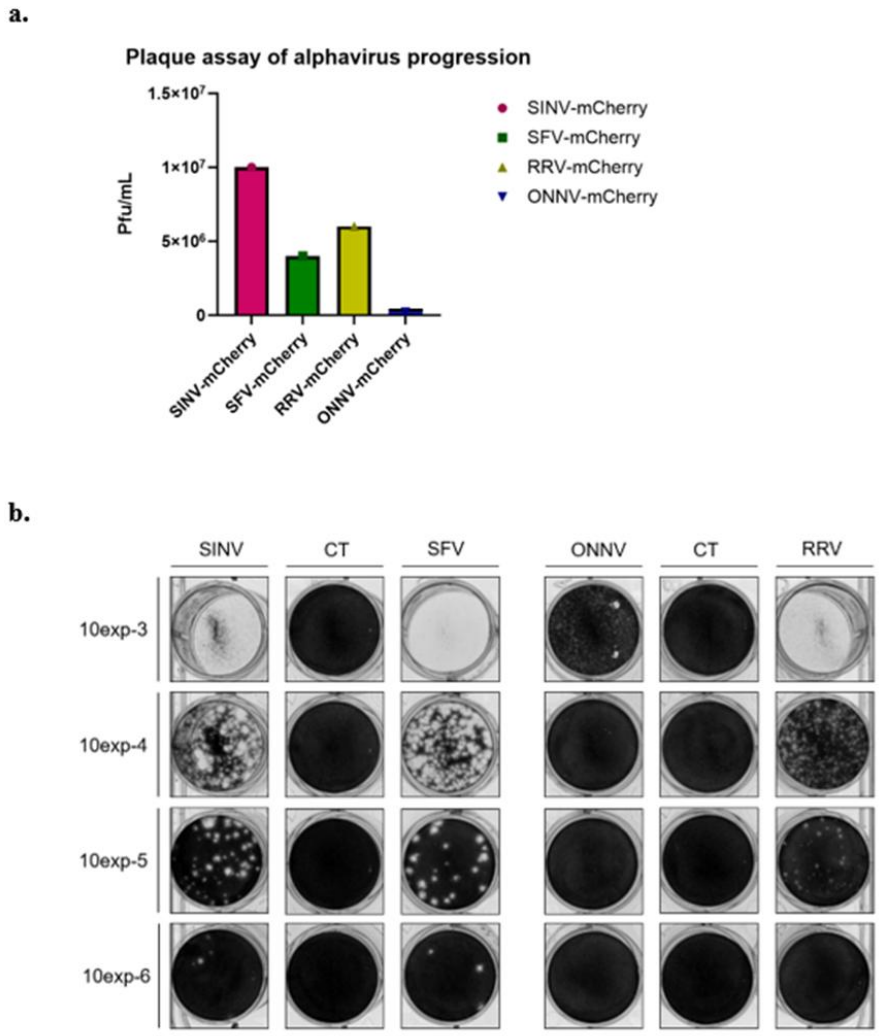

a. Viral titres of SINV-mCherry, SFV-mCherry, ONNV-mCherry, and RRV-mCherry were determined by plaque assay in Vero cells and expressed as plaque-forming units per millilitre (PFU/mL).
b. Representative wells used for viral titre determination. Vero cells were infected with serial dilutions of SINV-mCherry, SFV-mCherry, ONNV-mCherry or RRV-mCherry, and plaques were visualised following staining with crystal violet. CT, uninfected control. ONNV required an additional 20 h of plaque assay incubation for cytopathic effects to become apparent.

Sequential transfections were also evaluated (Table 1b, trials 8 and 9). Cells were treated with 25 nM siRNAs, followed by a second transfection with 25 nM or 50 nM siRNAs after 24 h. However, these conditions did not provide sufficiently consistent target protein depletion.

Finally, two siRNAs targeting the same protein were combined together at a total concentration of 50 nM and transfected using X-tremeGENE 360 for 48 h. This condition produced the most consistent depletion of U2AF1, U2AF2 and SF1 and was therefore used for subsequent knockdown experiments unless otherwise stated. Secondary trials on SFV and RRV were exploratory and are reported as feasibility rather than definitive phenotypes. (Supplementary Figure 4)

Figure 5: Initial optimisation of siRNA-mediated knockdown of U2AF1, U2AF2 and SF1.

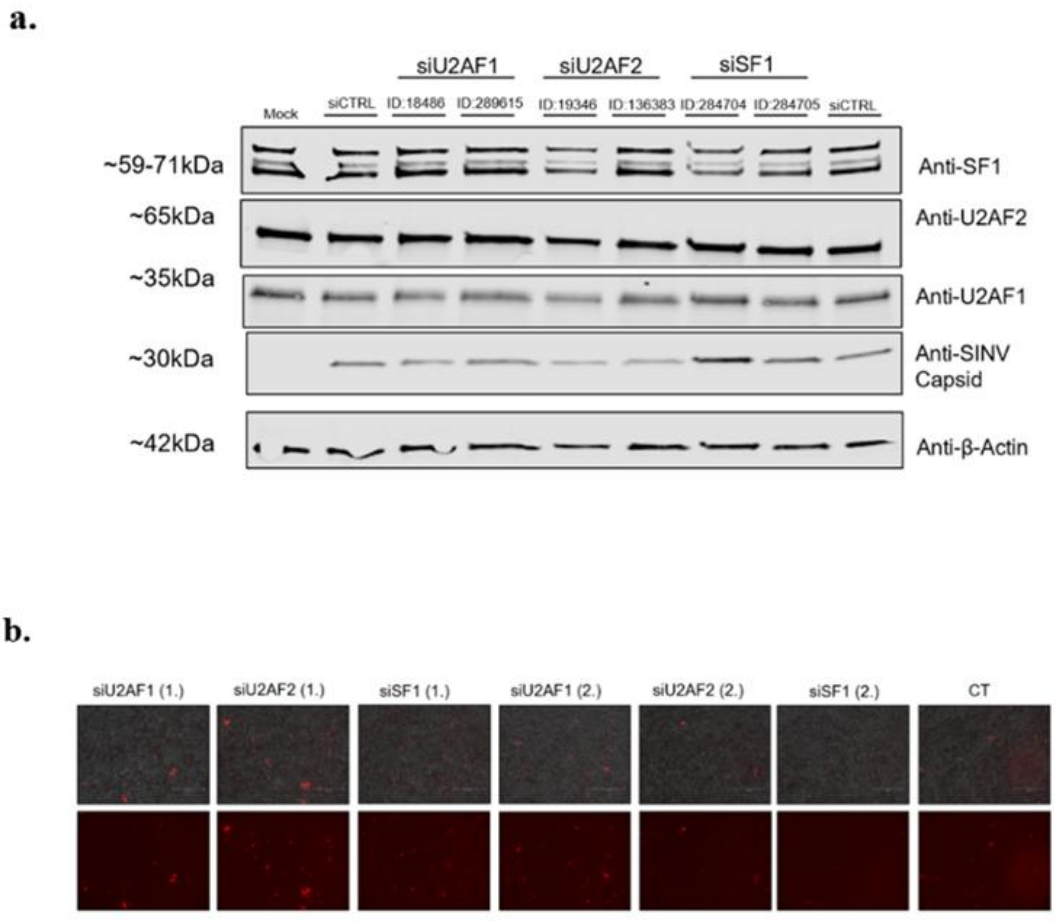

Figure 5 (On page 24):

a. Western blot analysis of U2AF1, U2AF2 and SF1 following 24 h transfection with two individual siRNAs targeting each protein. SINV capsid was detected as a marker of viral infection, and β-actin was used as a loading control. Knockdown of the target proteins was incomplete under these conditions.
b. Representative EVOS fluorescence images of SINV-mCherry infection following transfection with the individual siRNAs targeting U2AF1, U2AF2 or SF1. The upper panels show merged bright-field and mCherry fluorescence images, and the lower panels show the corresponding mCherry fluorescence channel. CT, control.

3.1.2 Replicate analysis of U2AF complex knockdown.

Three independent biological replicates of U2AF1, U2AF2, and SF1 knockdown experiments were performed using SINV-mScarlet at an MOI of 0.5 (Table 1b, trials 11–13). Viral replication was assessed by EVOS fluorescence microscopy, Western blot using capsid and mCherry antibodies, and plaque assays (Figures 6–7). These complementary assays were used to assess different aspects of the phenotype: Western blotting was used to evaluate protein depletion and viral protein expression, EVOS fluorescence microscopy to visualise reporter-virus infection, and plaque assays to quantify infectious viral titres. Western blot analysis showed consistent depletion of each target protein following treatment with the corresponding siRNAs across the three biological replicates (Figure 6).

Knockdown of U2AF1 consistently produced the largest effect shown in the plaque assay (Figure 7), resulting in an approximately 10-fold increase in SINV titres relative to control. This increase was statistically significant ($P = 0.0194$, unpaired two-tailed t-test with Welch's correction). SF1 knockdown led to an average 5-fold increase, but this did not reach statistical significance ($P = 0.1137$). In contrast, U2AF2 knockdown showed variable effects across replicates and no significant difference from control ($P = 0.2766$).

Together, these results support an antiviral role for U2AF1 during SINV infection, whereas the effects of SF1 and U2AF2 knockdown were not statistically significant under the conditions tested.

Figure 6 (on page 26):

Western blot of HEK293 cells transfected with siRNAs targeting U2AF1, U2AF2, or SF1 (n=3), or with a non-targeting control siRNA, followed by infection with nsP3-tagged SINV-mScarlet (MOI = 0.5). Cells were harvested at 18 h post-infection. U2AF1, U2AF2 and SF1 were detected to assess knockdown efficiency, while SINV capsid and mScarlet (by capsid and mCherry antibodies) were detected as markers of viral infection. β-actin was used as a loading control. Western blots from three independent biological replicates are shown (n = 3; Table 1b, trials 11–13).

Figure 6: Validation of siRNA-mediated knockdown of U2AF1, U2AF2 and SF1 during SINV infection.

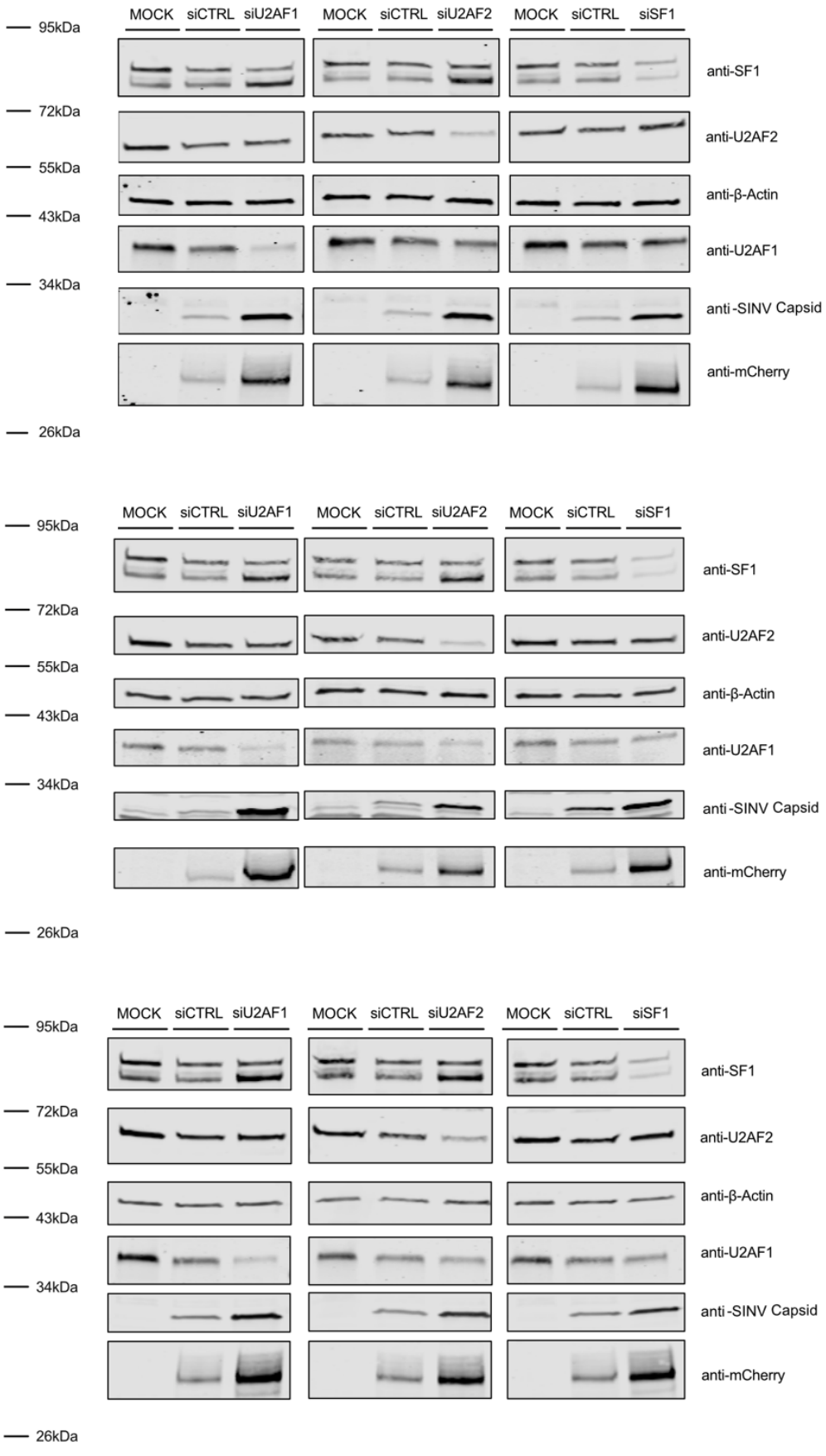

Figure 7. Effect of U2AF1, U2AF2 and SF1 knockdown on SINV infectious virus production.

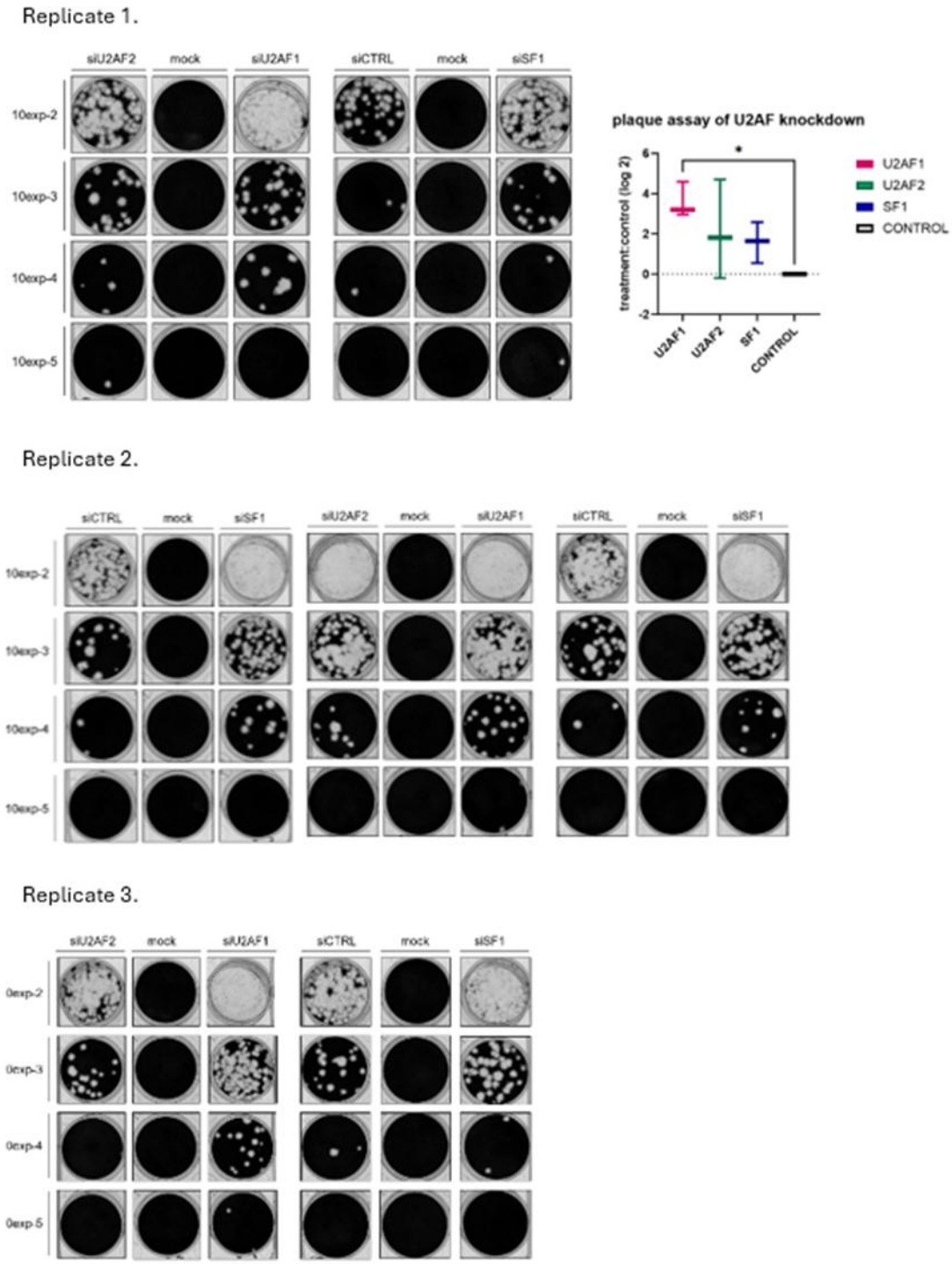

Plaque assays were performed to quantify infectious SINV-mScarlet titres in HEK293 cells following siRNA-mediated knockdowns of U2AF1, U2AF2, or SF1. Cells transfected with a non-targeting siRNA were used as controls. Cells were infected with nsP3-tagged SINV-mScarlet at an MOI of 0.5. The data correspond to the knockdown experiments shown in Figure 6 and represent three independent biological replicates (n = 3).

3.2.1 iCLIP2 protocol optimisation:

The siRNA knockdown experiment demonstrated that the components of the U2AF complex may influence SINV infection. U2AF1 knockdown produced a significant increase in viral titre, while SF1 knockdown showed a similar trend.
As these proteins are involved in RNA recognition during spliceosome assembly, we next investigated whether they interact with viral RNA during infection and whether such interactions occur at specific sites within the viral genome. To address this question, iCLIP2 was used to characterise protein–RNA interactions at high resolution. Immunoprecipitation was performed under iCLIP2 washing conditions, and antibody specificity was assessed by silver staining and Western blot (Figure 8), with IgG as a negative control and whole-cell lysate input as a positive control.

AQR, SF3B1, and SF1 showed clear enrichment by immunoprecipitation, with bands of the expected molecular weights confirmed by the corresponding Western blots in Figure 8, suggesting the suitability of these antibodies for the subsequent iCLIP2 protocol (Figure 3.). In contrast, silver staining of U2AF2 revealed additional bands, suggesting non-specific enrichment. To improve the specificity of U2AF2 immunoprecipitation, additional washing conditions were evaluated (Supplementary Figure 1).

U2AF1 immunoprecipitation did not produce a band corresponding to the expected molecular weight. Instead, the silver staining showed a band above 40 kDa, whereas U2AF1 was expected at approximately 35 kDa. The matching Western blot did not detect U2AF1, suggesting that the observed band was unlikely to represent U2AF1. U2AF1 was therefore excluded from subsequent iCLIP2 experiments (Figure 8 c).
The amount of whole-cell lysate required to achieve antibody-binding saturation was also optimised (Figure 8d). WCL volumes of 200 µL were sufficient for U2AF2, AQR and SF3B1, whereas 500 µL was required for SF1.

Based on these optimisation experiments, immunoprecipitation conditions were established for U2AF2, SF1, AQR and SF3B1, and these proteins were taken forward for subsequent iCLIP2 experiments.

Figure 8: Evaluation of antibodies for immunoprecipitation under iCLIP2 conditions

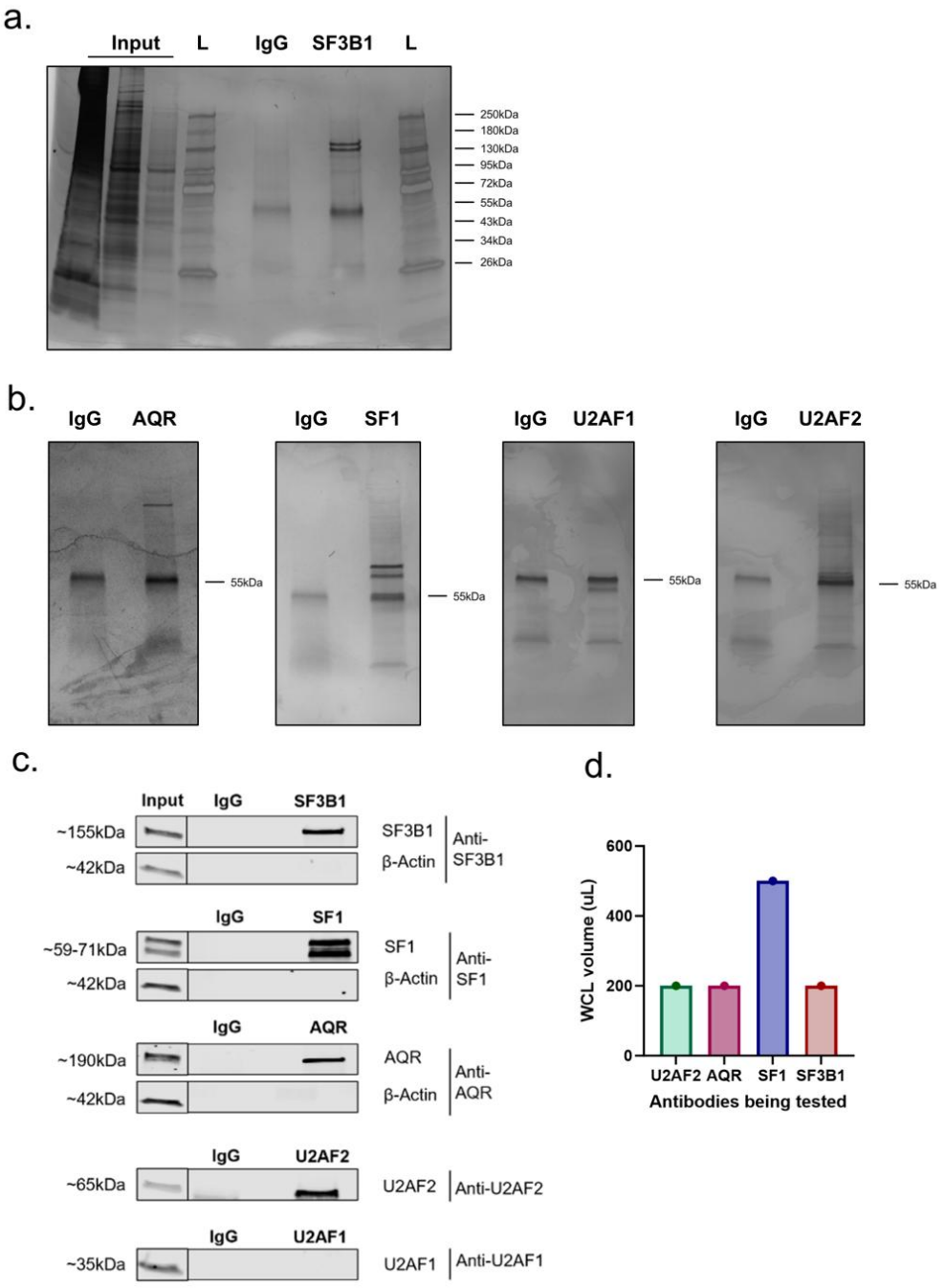

a. A Representative silver staining image following SF3B1 immunoprecipitation showing whole-cell lysate (input), IgG negative control and SF3B1 immunoprecipitation. L, protein ladder.
b. Silver staining demonstrates the immunoprecipitation for U2AF1, U2AF2, SF1, and AQR, with IgG immunoprecipitation included as a negative control.
c. Matching Western blot demonstrates the immunoprecipitation for: U2AF1, U2AF2, SF1, AQR and SF3B1. β-actin was used to assess non-specific enrichment where applicable. The band observed at approximately 55 kDa in the IgG samples corresponds to the IgG heavy chain.
d. Optimised whole-cell lysate (WCL) volumes used for immunoprecipitation with antibodies against U2AF2, AQR, SF1 and SF3B1. WCL volumes of 200 µL were used for U2AF2, AQR and SF3B1, whereas 500 µL was used for SF1.

3.2.2 UV and RNase dose optimisation:

Following optimisation of the immunoprecipitation conditions, UV-crosslinking and RNase treatment were further optimised for iCLIP2. Cells were initially exposed to 254 nm UV irradiation at 300 mJ, followed by RNase treatment at 10 U/mL according to the original protocol.

qPCR was used to assess the amount of amplifiable iCLIP2 library material recovered following library preparation. The quantification cycle (Cq) represents the PCR cycle at which the fluorescence signal reaches the detection threshold, with a lower Cq value indicating a greater amount of amplifiable starting material. In this experiment, successful UV-dependent enrichment of protein-associated RNA was therefore expected to result in a lower Cq value in the crosslinked sample than in the corresponding non-crosslinked control.
Under the initial 300 mJ crosslinking condition, only a limited difference in Cq values was observed between the crosslinked and non-crosslinked samples following SF3B1 immunoprecipitation (Figure 9a–d). This indicated that further optimisation of the RNase digestion and UV-crosslinking conditions was required.

RNase treatment was subsequently optimised to generate RNA fragments suitable for iCLIP2 library preparation. Different RNase concentrations were tested for SF3B1, SF1 and AQR immunoprecipitations (Figure 9 c, e–g). Among the conditions tested, RNase treatment at 10 U/mL (1:100 dilution) produced the strongest qPCR amplification signal and was therefore selected for subsequent experiments.

To examine whether increasing the energy in crosslinking would increase the amount of RNA extracted, we tested crosslinking at 300 mJ (Figure 9) and 600 mJ (Figure 10). Notably, compared to the Cq value in 300 mJ crosslinking (Figure 9d), at 600 mJ, a greater separation in Cq values between the crosslinked and non-crosslinked samples was observed than under the 300 mJ condition for most of the proteins (Figure 10b), consistent with greater recovery of crosslink-dependent RNA.
As the 300 and 600 mJ conditions were evaluated in separate optimisation experiments, absolute Cq values were not directly compared between the two experiments; instead, the difference between crosslinked and non-crosslinked samples within each experiment was

Figure 9: Optimisation of RNase treatment for iCLIP2 of SF3B1, SF1 and AQR.

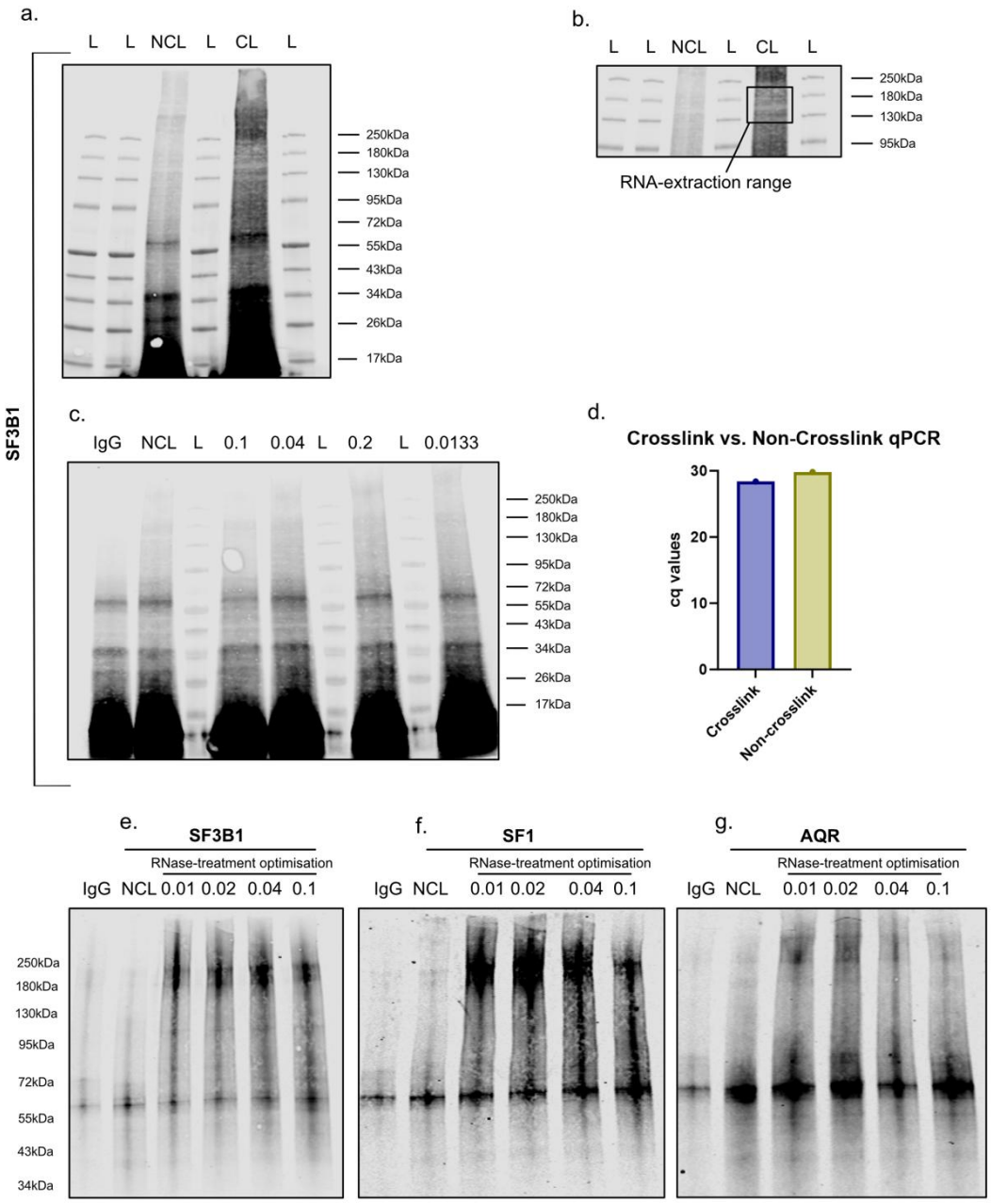

a. RNA smear associated with SF3B1 following immunoprecipitation and adaptor ligation, comparing non-crosslinked (NCL) and crosslinked (CL) samples. L, protein ladder.
b. SDS–PAGE gel illustrating the SF3B1 crosslinked sample, showing the molecular-weight range selected for RNA extraction during the initial optimisation.
c. Optimisation of imaging of RNase concentrations on RNA from SF3B1 immunoprecipitation, the RNase was diluted 1:10 (0.1), 1:25 (0.04), 1:50 (0.02), 1:75(0.0133). NCL, non-crosslinked control; L, protein ladder.
d. qPCR analysis comparing crosslinked and non-crosslinked samples from SF3B1 immunoprecipitation. Cq values are shown.
e~g. Optimisation of RNase treatment for (e) SF3B1, (f) SF1 and (g) AQR immunoprecipitations using RNase dilutions of 1:10 (0.1), 1:25 (0.04), 1:50 (0.02), and 1:100 (0.01). IgG and non-crosslinked (NCL) samples were included as controls.

considered. At 300 mJ, little separation was observed between crosslinked and non-crosslinked conditions. Following optimisation at 600 mJ, a clearer difference between crosslinked and non-crosslinked samples was observed.

The clearer separation observed at 600 mJ supported its use for subsequent iCLIP2 experiments. Based on the optimisation results, RNase treatment at 10 U/mL (1:100 dilution), and 600 mJ UV crosslinking were selected for subsequent experiments.

Figure 10: Optimisation of UV crosslinking at 600 mJ for iCLIP2.

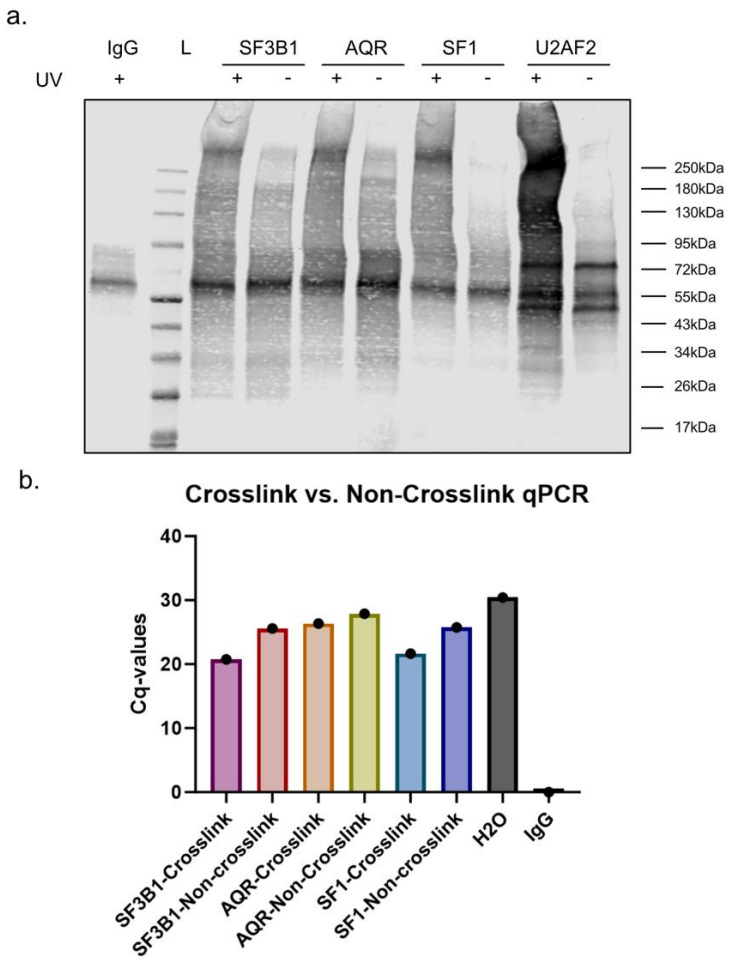

a. Smear detection when the UV-dose was increased to 600mJ. Comparison between crosslinked (+) and non-crosslinked (-) samples from SF3B1, AQR, SF1 and U2AF2. IgG immunoprecipitation was included as a negative control. L, protein ladder.

b. qPCR analysis of iCLIP2 libraries generated from crosslinked and non-crosslinked SF3B1, AQR and SF1 samples following UV irradiation at 600 mJ. Cq values represent the cycle at which the amplification signal reached the detection threshold, with lower Cq values indicating a greater amount of amplifiable library material. Crosslinked samples showed lower Cq values than their corresponding non-crosslinked controls. H_2O and IgG were included as negative controls.

3.2.3 cDNA generation and quality control:

Following optimisation of the iCLIP2 conditions, cDNA libraries were generated for AQR, SF3B1, U2AF2, and SF1, together with their corresponding SMI controls. Size-matched input regions were selected according to the molecular weights of the respective proteins. The input regions corresponding to SF3B1 and AQR were excised at approximately 130 kDa and designated SMI-130. The size-matched input for U2AF2 and SF1 was marked as SMI-55.

Following reverse transcription and library preparation, qPCR was performed on the iCLIP2-derived cDNA libraries from AQR, SF3B1, U2AF2 and SF1 immunoprecipitation samples and their corresponding size-matched input (SMI) controls. This served as a quality-control step to assess the amount of amplifiable library material and to determine the number of cycles required for PCR amplification (Figure 11).
A lower Cq value indicated a greater amount of amplifiable starting material. Differences in Cq values were observed between infected and mock-infected samples for the four immunoprecipitated proteins.

AQR showed a higher Cq value in infected samples than in mock-infected samples, whereas SF3B1 showed a lower Cq value following infection. Smaller differences were observed for SF1 and U2AF2 (Figure 11). These Cq values were used primarily for library quality control and optimisation of subsequent PCR amplification rather than as a direct measure of protein–RNA binding.
These results confirmed that amplifiable cDNA libraries were generated for AQR, SF3B1, U2AF2 and SF1 and were suitable for subsequent library amplification and quality assessment.

Figure 11: Quality control of iCLIP2 libraries by qPCR.

a.

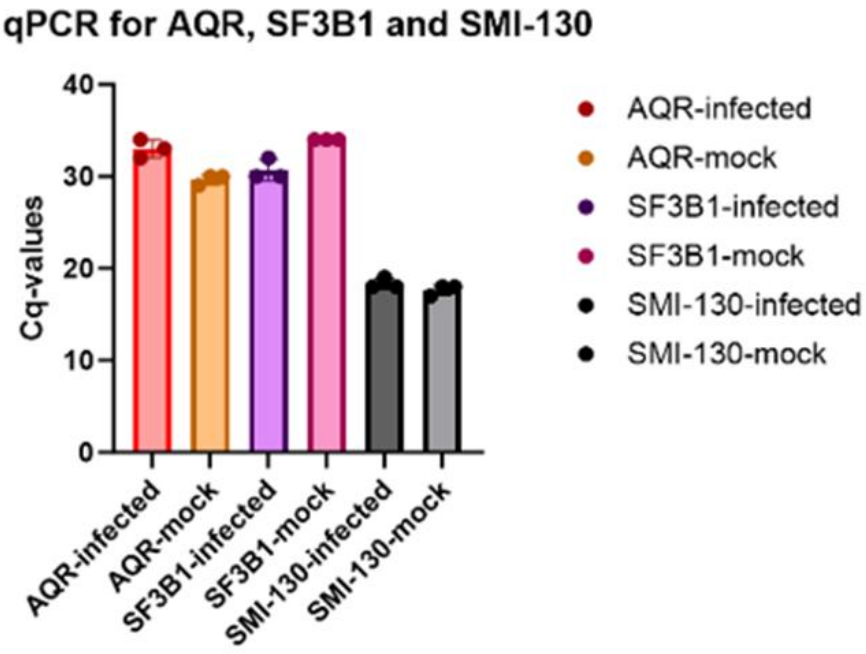

b.

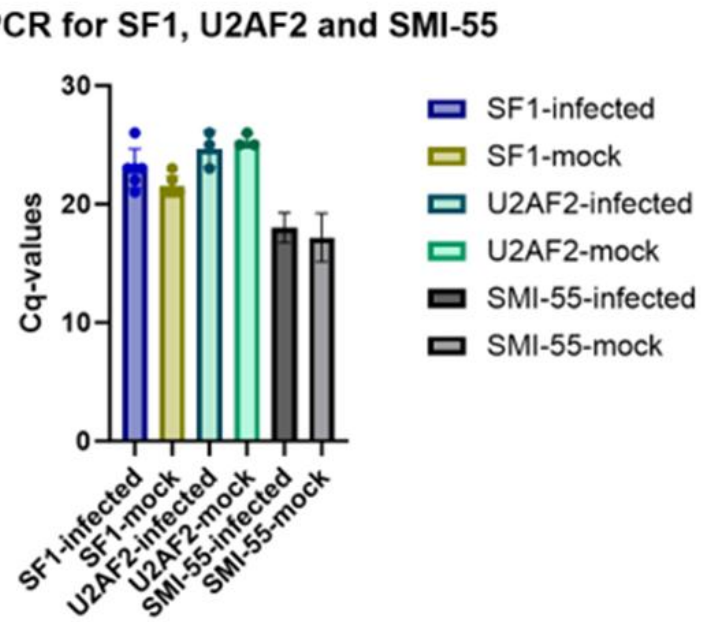

a. Cq values of iCLIP2 libraries generated from AQR, SF3B1 immunoprecipitation samples and their corresponding size-matched input (SMI-130) controls. Infected and mock-infected samples are shown for each condition.
b. Cq values of iCLIP2 libraries generated from SF1 and U2AF2 immunoprecipitation samples and their corresponding size-matched input (SMI-55) controls. Infected and mock-infected samples are shown for each condition. Lower Cq values indicate a greater amount of amplifiable library material.

3.2.3 cDNA generation and quality control:

Following optimisation of the iCLIP2 conditions, cDNA libraries were generated for AQR, SF3B1, U2AF2, and SF1, together with their corresponding SMI controls. Size-matched input regions were selected according to the molecular weights of the respective proteins. The input regions corresponding to SF3B1 and AQR were excised at approximately 130 kDa and designated SMI-130. The size-matched input for U2AF2 and SF1 was marked as SMI-55.

Following reverse transcription and library preparation, qPCR was performed on the iCLIP2-derived cDNA libraries from AQR, SF3B1, U2AF2 and SF1 immunoprecipitation samples and their corresponding size-matched input (SMI) controls. This served as a quality-control step to assess the amount of amplifiable library material and to determine the number of cycles required for PCR amplification (Figure 11). A lower Cq value indicated a greater amount of amplifiable starting material. Differences in Cq values were observed between infected and mock-infected samples for the four immunoprecipitated proteins.

AQR showed a higher Cq value in infected samples than in mock-infected samples, whereas SF3B1 showed a lower Cq value following infection. Smaller differences were observed for SF1 and U2AF2 (Figure 11). These Cq values were used primarily for library quality control and optimisation of subsequent PCR amplification rather than as a direct measure of protein–RNA binding.

These results confirmed that amplifiable cDNA libraries were generated for AQR, SF3B1, U2AF2 and SF1 and were suitable for subsequent library amplification and quality assessment.

3.2.4 Library size determination and reverse size selection:

To assess library size distribution and ensure equalisation before sequencing, a Tapestation analysis was performed (Supplementary Figure 2). Libraries with the expected size distribution contained a substantial proportion of fragments within a 100–300 bp range.

Samples in which less than 40% of the library signal fell within this range were subjected to an additional reverse size-selection step.
The data in Supplementary Figure 2 and Supplementary Table 1, as well as the distribution pattern in Figure 12, demonstrate that one sample (R3_mock_SMI55) showed an abnormally broad fragment-size distribution with substantial high-molecular-weight DNA and little material within the expected 100–300 bp range (Figure 12, c). Several other samples, including R2_mock_SF3B1, R2_infected_AQR, R1_infected_SF3B1, R3_infected_AQR, R5_infected_U2AF2, R1_infected_AQR and R1_mock_SMI130, contained less than 40% of their library signal within the expected 100–300 bp range. An example of a library containing an excess of larger DNA fragments is shown in Figure 12, b.

Because an excess of large DNA fragments could interfere with subsequent library pooling and sequencing, unsatisfied samples were processed with reverse size selection. Following reverse size selection, the proportion of library material within the desired size range increased by approximately 8 percentage points across the affected samples (Supplementary Figure 3, Supplementary Table 2).

Overall, the optimisation experiments established conditions for generating iCLIP2 libraries for AQR, SF3B1, U2AF2, and SF1 under both infected and uninfected conditions. The libraries were submitted for sequencing, with subsequent analysis planned in collaboration with the CVR bioinformatics group.

3.2.5 Summary of results:

In summary, the first section of this project demonstrated that U2AF1 knockdown enhanced SINV replication, supporting an antiviral role of U2AF1. SF1 knockdown showed a similar trend towards increased viral replication, it did not reach statistical significance, whereas U2AF2 showed variable effects during siRNA knockdown studies.
In the second section, the iCLIP2 optimisation yielded sequencing-ready libraries for SF1, SF3B1, AQR and U2AF2 under SINV-infected and mock-infected conditions.

Figure 12. Representative iCLIP2 library size distribution profiles assessed by TapeStation.

a.

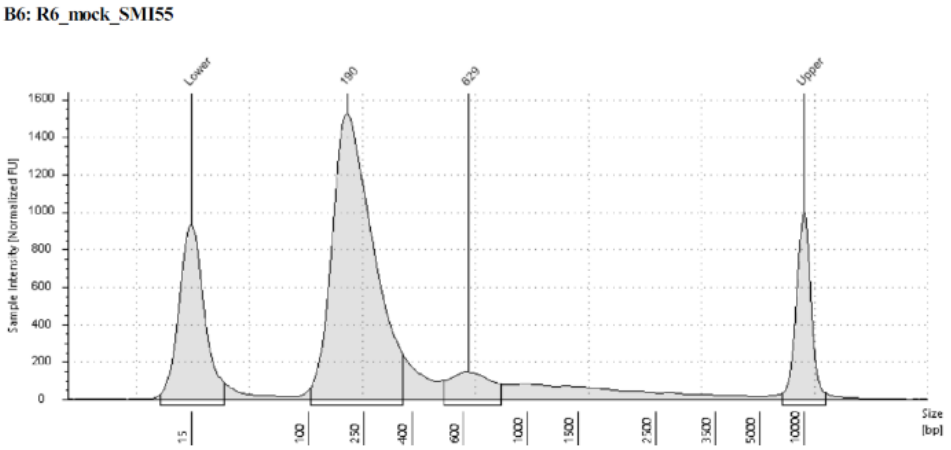

b.

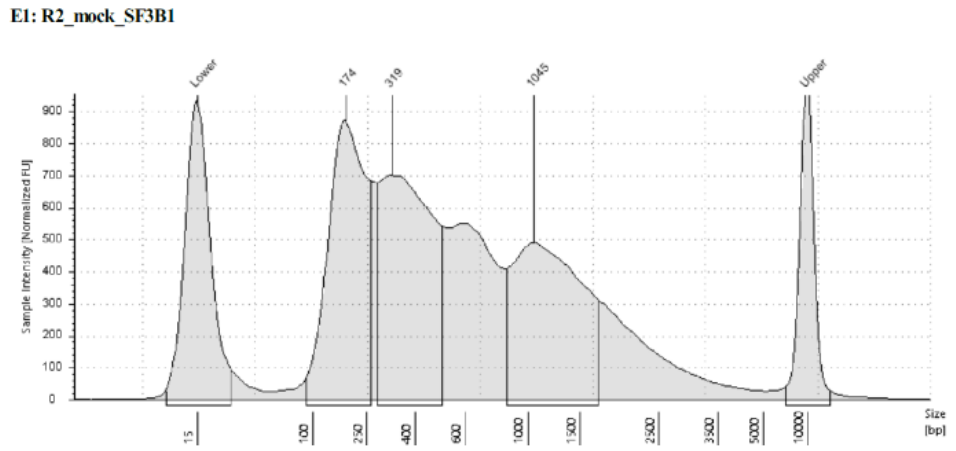

c.

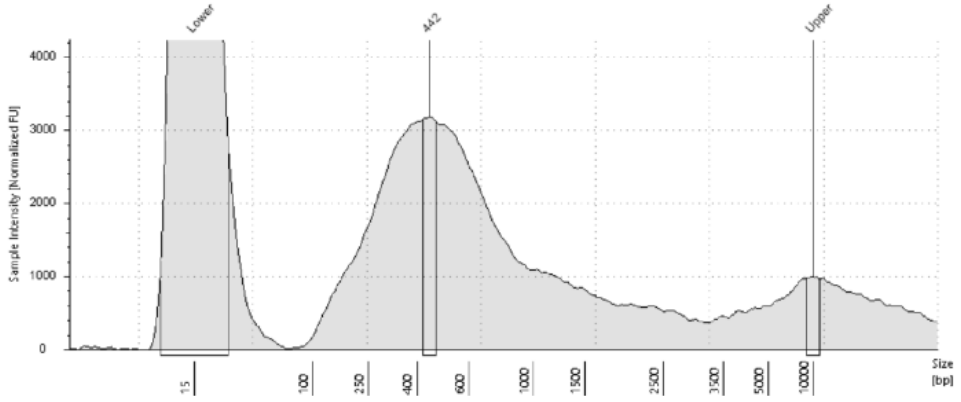

a. Representative library with the majority of fragments within the expected size range of approximately 100–300 bp (R6_MOCK_SMI55).
b. Representative library containing an excess of large fragments (R2_MOCK_SF3B1), which was subsequently subjected to reverse size selection.
c. Representative sample showing an abnormal broad fragment-size distribution with substantial high-molecular-weight DNA (R3_MOCK_SMI55), indicating unsuccessful library preparation.

PART 4: DISCUSSION

4.1 The antiviral roles of the U2AF complex.

Our results support a potential antiviral role for components of the U2AF complex, comprising U2AF1, U2AF2 and SF1, during SINV infection. U2AF1 knockdown produced the strongest and most consistent increase in SINV titre, whereas SF1 knockdown showed a similar trend towards increased viral replication, although this did not reach statistical significance. In contrast, U2AF2 knockdown produced more variable effects across biological replicates.

This result extended the observations of Kamel et al., who reported that the U2 snRNP suppresses viral replication through interactions with viral RNA. The U2AF complex functions upstream of U2 snRNP recruitment during early spliceosome assembly. Therefore, our findings raise the possibility that the components of the U2AF complex may contribute to antiviral functions at an early stage, either before or concurrently with the recruitment of the U2 snRNP and its associated SF3B complex.

Plaque assay analysis showed that U2AF1 knockdown produced the largest increase in SINV titre relative to the siRNA control, followed by SF1 knockdown, whereas the effect of U2AF2 knockdown was less consistent.

U2AF1 and U2AF2 form a heterodimer and are functionally interconnected. Shao et al. (2014) reported that the depletion of U2AF2 also led to a reduction in U2AF1, whereas the knockdown of U2AF1 did not affect U2AF2 expression[11]. Warnasooriya et al. (2020) further demonstrated that U2AF1 can stabilise U2AF2 and alter its conformation during intron binding[26]. Furthermore, in Palangat et al.'s study (2019), the U2AF heterodimer translocated to the cytoplasm in the absence of infection. Although U2AF1 binding sites were associated with U2AF2 footprints, immunoprecipitation of crosslinked U2AF1–RNP complexes did not co-precipitate U2AF2. The variable phenotype observed following U2AF2 knockdown may instead reflect insufficient or inconsistent U2AF2 depletion, and further experiments with quantitative validation of knockdown efficiency would be required to establish its role in SINV replication.

Nevertheless, previous studies suggest that U2AF2 can have context-dependent functions during viral infection. In our RRV infection trial (Supplementary Figure 4),

U2AF2 knockdown was associated with enhanced viral replication, although this observation requires validation in additional biological replicates. For example, Yuan et al. (2024) showed that JEV, a positive-sense single-stranded RNA flavivirus, hijacks cytoplasmic U2AF2 to promote its replication. These observations raise the possibility that U2AF2 may have context-dependent roles during viral infection, potentially contributing to antiviral restriction in some settings while being exploited by viruses in others. Another possibility is that the U2AF complex recognises different viral sequences or structures within viral RNAs as its binding sites, leading to different effects in viral progression; however, this hypothesis will require direct investigation of the viral RNA-binding profiles of U2AF proteins. Further experiments with validated U2AF2 depletion will be required to determine whether the variable effects observed here reflect a virus-specific function or insufficient knockdown efficiency.

Taken together, we hypothesise that U2AF1 and U2AF2 may have distinct but potentially cooperative functions during viral infection:

- U2AF1 may contribute directly to antiviral restriction, although the underlying mechanism remains to be determined.
- The contribution of U2AF2 remains unclear because its knockdown produced variable effects, and the extent of depletion may have been insufficient to reveal a reproducible viral phenotype.
- Previous studies suggest that U2AF1 and U2AF2 can have both cooperative and independent functions, providing potential mechanisms that could be investigated in future studies.

4.2 The optimisation of iCLIP2.

iCLIP2 libraries for SF3B1, SF1, U2AF2 and AQR were successfully generated and were suitable for sequencing.

The previous functional assays indicated that, in addition to the U2 snRNP, components of the U2AF complex may contribute to antiviral activity during SINV infection. This raised the question of whether these proteins directly recognise specific sequences within viral RNA. To achieve this, iCLIP2 experimental conditions were optimised for U2AF2, SF1, SF3B1, and AQR. Optimisation included varying lysate concentration,

RNase digestion and crosslinking energy to establish suitable conditions for library preparation.

During these trials, the U2AF1 antibody consistently produced non-specific signals. We also tested U2AF1 immunoprecipitation using another antibody; however, we were unable to identify an antibody suitable for endogenous U2AF1 CLIP. Indeed, most published U2AF1 CLIP studies have relied on tagged U2AF1. For example, Shao et al. (2014) and Palangat et al. (2019) expressed tagged U2AF1 and used anti-tag antibodies for immunoprecipitation. Difficulties with endogenous U2AF1 immunoprecipitation have also been reported; for example, two different U2AF1 antibodies (Bethyl Laboratories, A302-079 and A302-080) failed to pull down the protein individually.[31] These observations suggest that the inability to generate U2AF1 iCLIP2 libraries in the present study may reflect technical limitations associated with endogenous U2AF1 immunoprecipitation.

In addition to U2AF1, U2AF2 presented challenges during antibody validation. Silver staining following U2AF2 immunoprecipitation contained numerous background bands, potentially reflecting its stable protein–protein interactions that were not fully disrupted by our high-salt wash conditions. Future studies could explore increasing NaCl concentration and performing additional washes to improve specificity. According to the BioGRID Database of Protein, Genetic, and Chemical Interactions retrieved on September 11th, 2025[30], U2AF2 was reported to have 657 identical interactors, more than SF3B1, which had the second-highest number among the proteins examined. Both U2AF2 and SF3B1 had more reported interactors than SF1, AQR and U2AF1. Optimisation of the washing conditions reduced non-specific signals, supporting the idea that U2AF2 associates with many other proteins, consistent with U2AF2 participating in an extensive protein-interaction network.

Interestingly, qPCR analysis revealed differences between SINV-infected and non-infected samples for AQR and SF3B1. AQR showed higher Cq values following SINV infection, whereas SF3B1 showed lower Cq values. As lower Cq values indicate a greater amount of amplifiable starting material, these differences may reflect changes in the amount of recovered protein-associated RNA. However, Cq values alone cannot establish changes in protein–RNA binding, and sequencing analysis will be required to determine whether SINV infection alters the RNA-binding profiles of AQR and SF3B1.

Given that AQR functions at a later stage of spliceosome assembly, whereas SF3B1 acts earlier, these differences are of potential interest. This observation may also be considered in the context of Kamel et al. (2024), who reported that SF3B1 localises to the cytoplasm under non-infected conditions, whereas AQR only appears in the cytoplasm following infection. Together, these observations raise the possibility that alphavirus infection differentially affects spliceosomal proteins at different stages of spliceosome assembly, although further analysis of the iCLIP2 sequencing data will be required to determine whether these differences are associated with altered viral RNA binding.

4.3 Limitations:

Biological limitations:

This project was conducted to explore the U2AF complex's antiviral effect during alphavirus infection; thus, further exploration is required to determine whether these effects extend to other viruses. We established experimental conditions for RRV; however, due to time constraints, biological replicates for ONNV, RRV, and SFV were not completed. Regarding the U2AF2 phenotype presented in our plaque assays and discussed in Section 4.1, further experiments with other RNA viruses are needed to clarify whether U2AF2 acts as a restriction factor or can be co-opted to support viral replication.

Additionally, although knockdown of SF1 reproducibly led to an increase in viral titres, the effect did not reach statistical significance. This limits our ability to conclude whether SF1 functions as a bona fide restriction factor. Larger sample sizes or complementary experimental approaches will be required to clarify the role of SF1 in alphavirus infection.

In summary, the current results do not provide sufficient evidence to establish U2AF2 as a consistent antiviral restriction factor. Future studies should therefore examine a broader range of single-stranded RNA viruses and additional cellular models, including primary cells, to determine whether the observed effects are virus- or cell-type-dependent.

Mechanistic limitations:

In this project, we aimed to investigate mechanistic insight by identifying U2AF complex candidates that may contribute to viral RNA recognition. We initially hypothesised that the U2AF complex might activate canonical interferon pathways; however, evidence from Tapescu et al. (2023) indicates that other splicing proteins, such as DDX39A, can restrict viruses independently of interferon. This raises the question of whether U2AF-mediated antiviral activity is dependent on interferon signalling. Importantly, cell line context complicates this interpretation: Chen et al. (2025) reported that HEK293T cells are deficient in interferon expression[33], whereas HEK293 cells, which were the primary model in our knockdown and iCLIP2 experiments, have a competent innate immunity.

This distinction suggests that repeating knockdowns in HEK293T with the same knockdown assay would help to investigate whether the antiviral phenotypes observed following U2AF complex knockdown are dependent on interferon signalling. Additionally, the inability to identify a suitable U2AF1 antibody for iCLIP2 limited our ability to investigate the RNA-binding profile of U2AF1 and therefore prevented a complete comparison of the candidate proteins examined in this study.

Technical limitations

During optimisation of the iCLIP2 protocol, increasing the UV dose to 600 mJ enhanced the recovery of crosslinked material under our experimental conditions. However, this dose is higher than the 400 mJ UV used in the eCLIP protocol[35, 36]. A higher dose of UV may increase RNA damage, which might affect the accuracy of our library quality and representation.

In addition, during iCLIP2 amplification, excessive PCR cycling of AQR and SF3B1 samples resulted in the accumulation of artefactual long DNA fragments, potentially caused by daisy-chaining of PCR products. Such artefacts can compromise sequencing quality and hinder downstream data interpretation.

Mitigation:

1. Extend knockdown assays to other alphaviruses (ONNV, RRV, SFV) and representative non-alphavirus RNA viruses.
2. Test antiviral phenotypes in additional cell lines and in primary cells.
3. Re-test U2AF2's role across different viral families to clarify whether it functions as a restriction factor or can be exploited by viruses.

4.4 Conclusion:

In conclusion, the findings of this project support an antiviral role for components of the U2AF complex during SINV infection, particularly U2AF1, while highlighting their potential roles for further investigation in other alphaviruses.
This project also optimised the iCLIP2 protocol and generated iCLIP2 libraries for AQR, SF3B1, U2AF2, and SF1 under both infected and uninfected conditions. These libraries are now in the process of being pooled and sequenced. The resulting data will enable the investigation of how the RNA-binding profiles of these proteins change upon infection and which specific sequences within viral RNA are recognised. This will provide a basis for investigating the mechanisms underlying the potential antiviral functions of these splicing-associated proteins.

All in all, this work highlights the potential contributions of the U2AF complex components to viral restriction and establishes a foundation for future studies to define their functions and dissect protein–RNA interactions.

REFERENCE:

1. Choquet, K., Patop, I.L. & Churchman, L.S. (2025). The regulation and function of post-transcriptional RNA splicing. *Nat Rev Genet*, **26**, 378–394. https://doi.org/10.1038/s41576-025-00836-z
2. Wuarin, J. & Schibler, U. (1994). Physical isolation of nascent RNA chains transcribed by RNA polymerase II: evidence for cotranscriptional splicing. *Mol Cell Biol*, **14**(11), 7219–7225. https://doi.org/10.1128/mcb.14.11.7219-7225.1994
3. Herzel, L., Ottoz, D., Alpert, T. & Neugebauer, K.M. (2017). Splicing and transcription touch base: co-transcriptional spliceosome assembly and function. *Nat Rev Mol Cell Biol*, **18**, 637–650. https://doi.org/10.1038/nrm.2017.63
4. Rogalska, M.E., Vivori, C. & Valcárcel, J. (2023). Regulation of pre-mRNA splicing: roles in physiology and disease, and therapeutic prospects. *Nat Rev Genet*, **24**, 251–269. https://doi.org/10.1038/s41576-022-00556-8
5. de Almeida, R.A. & O'Keefe, R.T. (2015). The NineTeen Complex (NTC) and NTC-associated proteins as targets for spliceosomal ATPase action during pre-mRNA splicing. *RNA Biol*, **12**(2), 109–114. https://doi.org/10.1080/15476286.2015.1008926
6. Chen, W. & Moore, M.J. (2015). Spliceosomes. *Curr Biol*, **25**(5), R181–R183. https://doi.org/10.1016/j.cub.2014.11.059
7. Sparks, M.E. & Brendel, V. (2005). Incorporation of splice site probability models for non-canonical introns improves gene structure prediction in plants. *Bioinformatics*, **21**(Suppl_3), iii20–iii30. https://doi.org/10.1093/bioinformatics/bti1205
8. Sibley, C.R., Blazquez, L. & Ule, J. (2016). Lessons from non-canonical splicing. *Nat Rev Genet*, **17**, 407–421. https://doi.org/10.1038/nrg.2016.46
9. Yin, Y., Lu, J.Y., Zhang, X. et al. (2020). U1 snRNP regulates chromatin retention of noncoding RNAs. *Nature*, **580**, 147–150. https://doi.org/10.1038/s41586-020-2105-3
10. Bak-Gordon, P. & Manley, J.L. (2025). SF3B1: from core splicing factor to oncogenic driver. *RNA*, **31**(3), 314–332. https://doi.org/10.1261/rna.080368.124
11. Shao, C., Yang, B., Wu, T. et al. (2014). Mechanisms for U2AF to define 3' splice sites and regulate alternative splicing in the human genome. *Nat Struct Mol Biol*, **21**, 997–1005. https://doi.org/10.1038/nsmb.2906
12. Schlackow, M., Nojima, T., Gomes, T., Dhir, A., Carmo-Fonseca, M. & Proudfoot, N.J. (2017). Distinctive patterns of transcription and RNA processing for human lincRNAs. *Mol Cell*, **65**(1), 25–38. https://doi.org/10.1016/j.molcel.2016.11.029
13. Kim, A.S. & Diamond, M.S. (2023). A molecular understanding of alphavirus entry and antibody protection. *Nat Rev Microbiol*, **21**, 396–407. https://doi.org/10.1038/s41579-022-00825-7
14. Kril, V., Hons, M., Amadori, C. et al. (2024). Alphavirus nsP3 organizes into tubular scaffolds essential for infection and the cytoplasmic granule architecture. *Nat Commun*, **15**, 8106. https://doi.org/10.1038/s41467-024-51952-z
15. Lloyd, R.E. (2015). Nuclear proteins hijacked by mammalian cytoplasmic plus strand RNA viruses. *Virology*, **479–480**, 457–474. https://doi.org/10.1016/j.virol.2015.03.001
16. Yuan, H., Zou, J.H., Luo, Y. et al. (2024). Cellular nuclear-localized U2AF2 protein is hijacked by the flavivirus 3'UTR for viral replication complex formation and RNA synthesis. *Vet Microbiol*, **290**, 109977. https://doi.org/10.1016/j.vetmic.2023.109977
17. Kamel, W., Ruscica, V., Embarc-Buh, A. et al. (2024). Alphavirus infection triggers selective cytoplasmic translocation of nuclear RBPs with moonlighting antiviral roles. *Mol Cell*, **84**(24), 4896–4911.e7. https://doi.org/10.1016/j.molcel.2024.11.015
18. Castello, A. & Kamel, W. (2025). Nuclear RNA-binding proteins meet cytoplasmic viruses. *RNA*, **31**(3), 444–451. https://doi.org/10.1261/rna.080313.124
19. Tapescu, I., Taschuk, F., Pokharel, S.M. et al. (2023). The RNA helicase DDX39A binds a conserved structure in chikungunya virus RNA to control infection. *Mol Cell*, **83**(22), 4174–4189.e7. https://doi.org/10.1016/j.molcel.2023.10.008
20. Roche. (n.d.). X-tremeGENE™ 360 Transfection Reagent. Sigma-Aldrich. Accessed July 1, 2025. Available at: https://www.sigmaaldrich.com/GB/en/product/roche/xtg360ro
21. Zhan, X., Lu, Y. & Shi, Y. (2024). Molecular basis for the activation of human spliceosome. *Nat Commun*, **15**, 6348. https://doi.org/10.1038/s41467-024-50785-0

22. Thermo Fisher Scientific. (n.d.). SilverQuest™ Silver Staining Kit: Instruction manual. Accessed July 1, 2025. Available at: https://assets.fishersci.com/TFS-Assets/LSG/manuals/silverquest_man.pdf
23. Zymo Research. (n.d.). Zymo-Spin IC columns. Accessed July 9, 2025. Available at: https://www.zymoresearch.com/products/zymo-spin-ic-columns
24. Thiruvaiyaru, A., Mattila, S., Sadeghi, M. et al. (2025). Proximity interactome of alphavirus replicase component nsP3 includes proviral host factors eIF4G and AHNAK. *PLoS Pathog*, **21**(4), e1013050. https://doi.org/10.1371/journal.ppat.1013050
25. Palangat, M., Anczuków, O., Krainer, A.R. et al. (2019). The splicing factor U2AF1 contributes to cancer progression through a noncanonical role in translation regulation. *Genes Dev*, **33**(9–10), 482–497. https://doi.org/10.1101/gad.322719.118
26. Warnasooriya, C., Feeney, C.F., Laird, K.M. et al. (2020). A splice site-sensing conformational switch in U2AF2 is modulated by U2AF1 and its recurrent myelodysplasia-associated mutation. *Nucleic Acids Res*, **48**(10), 5695–5709. https://doi.org/10.1093/nar/gkaa293
27. Khan, S., Tang, Y., Guo, Y. et al. (2025). Revealing the role of U2AF1 in splicing regulation and chimeric RNA dynamics. *Sci Rep*, **15**, 16235. https://doi.org/10.1038/s41598-025-99865-1
28. Esfahani, M.S., Lee, L.J., Jeon, Y.J. et al. (2019). Functional significance of U2AF1 S34F mutations in lung adenocarcinomas. *Nat Commun*, **10**, 5712. https://doi.org/10.1038/s41467-019-13392-y
29. Oughtred, R., Rust, J., Chang, C. et al. (2021). The BioGRID database: a comprehensive biomedical resource of curated protein, genetic and chemical interactions. *Nucleic Acids Res*, **49**(D1), D1234–D1246. https://doi.org/10.1093/nar/gkaa1113
30. BioGRID. (n.d.). U2AF2 Homo sapiens (human) Summary. Accessed July 10, 2025. Available at: https://thebiogrid.org/116466
31. Kwon, Y.S., Jin, S.W., Song, H. et al. (2024). Global analysis of binding sites of U2AF1 and ZRSR2 reveals RNA elements required for mutually exclusive splicing by the U2- and U12-type spliceosome. *Nucleic Acids Res*, **52**(3), 1420–1434. https://doi.org/10.1093/nar/gkad1180
32. Buchbender, A., Mutter, H., Sutandy, F.X.R. et al. (2020). Improved library preparation with the new iCLIP2 protocol. *Methods*, **178**, 33–48. https://doi.org/10.1016/j.ymeth.2019.10.003
33. Chen, H., Charles, P.D., Gu, Q. et al. (2025). Omics analyses uncover host networks defining virus-permissive and -hostile cellular states. *Mol Cell Proteomics*, **24**(5), 100966. https://doi.org/10.1016/j.mcpro.2025.100966
34. Zarnegar, B., Flynn, R.A., Shen, Y. et al. (2016). irCLIP platform for efficient characterization of protein–RNA interactions. *Nat Methods*, **13**, 489–492. https://doi.org/10.1038/nmeth.3840
35. Van Nostrand, E. & Yeo, G. (2019). UV crosslinking of suspension cells for eCLIP. *protocols.io*. https://doi.org/10.17504/protocols.io.z62f9ge
36. Van Nostrand, E.L., Pratt, G.A., Shishkin, A.A. et al. (2016). Robust transcriptome-wide discovery of RNA-binding protein binding sites with enhanced CLIP (eCLIP). *Nat Methods*, **13**(6), 508–514. https://doi.org/10.1038/nmeth.3810
37. Schlesinger, S. & Schlesinger, M. J. (1996). In *Field's Virology*, 3rd ed. (ed. B. N. Fields et al.), 825–843. Lippincott-Raven Publishers, Philadelphia.
38. Garcia-Moreno, M., Sanz, M. & Carrasco, L. (2016). A viral mRNA motif at the 3'-untranslated region that confers translatability in a cell-specific manner: Implications for virus evolution. *Sci Rep*, 6, 19217. https://doi.org/10.1038/srep19217
39. Kuhn, R. J., Hong, Z. & Strauss, J. H. (1990). Mutagenesis of the 3' nontranslated region of Sindbis virus RNA. *J Virol*, 64, 1465–1476.
40. Dickson, A. M. et al. (2012). Dephosphorylation of HuR protein during alphavirus infection is associated with HuR relocalization to the cytoplasm. *J Biol Chem*, 287, 36229–36238.

Supplementary item	Related main-text section
Oligonucleotide sequences	Methods 2.9.8
Supplementary Figure 1	Results 3.2.1, validation of Western blot quantification
Supplementary Figure 2	Results 3.2.4
Supplementary Table 1	
Supplementary Figure 3	
Supplementary Table 2	
Supplementary Figure 4	Results 3.1.1
Supplementary Table 3	Materials 2

Oligonucleotide sequences used in iCLIP2

RT-Oligo used for reverse transcription.
GGATCCTGAACCGCT

L3-App
/rApp/AGATCGGAAGAGCGGTTCAG/ddC/

L01clip2.0
/5Phos/NNNNATCACGNNNNNAGATCGGAAGAGCGTCGTG/3ddC/

L02clip2.0
/5Phos/NNNNCGATGTNNNNNAGATCGGAAGAGCGTCGTG/3ddC/

L03clip2.0
/5Phos/NNNNTTAGGCNNNNNAGATCGGAAGAGCGTCGTG/3ddC/

L04clip2.0
/5Phos/NNNNTGACCANNNNNAGATCGGAAGAGCGTCGTG/3ddC/

L05clip2.0
/5Phos/NNNNACAGTGNNNNNAGATCGGAAGAGCGTCGTG/3ddC/

L06clip2.0
/5Phos/NNNNGCCAATNNNNNAGATCGGAAGAGCGTCGTG/3ddC/

L07clip2.0
/5Phos/NNNNCAGATCNNNNNAGATCGGAAGAGCGTCGTG/3ddC/

L08clip2.0
/5Phos/NNNNACTTGANNNNNAGATCGGAAGAGCGTCGTG/3ddC/

L09clip2.0
/5Phos/NNNNGATCAGNNNNNAGATCGGAAGAGCGTCGTG/3ddC/

L10clip2.0
/5Phos/NNNNTAGCTTNNNNNAGATCGGAAGAGCGTCGTG/3ddC/

L11clip2.0
/5Phos/NNNNATGAGCNNNNNAGATCGGAAGAGCGTCGTG/3ddC/

L12clip2.0
/5Phos/NNNNCTTGTANNNNNAGATCGGAAGAGCGTCGTG/3ddC/

L13clip2.0
/5Phos/NNNNAGTCAANNNNNAGATCGGAAGAGCGTCGTG/3ddC/

L14clip2.0
/5Phos/NNNNAGTTCCNNNNNAGATCGGAAGAGCGTCGTG/3ddC/

L15clip2.0
/5Phos/NNNNATGTCANNNNNAGATCGGAAGAGCGTCGTG/3ddC/

L16clip2.0
/5Phos/NNNNCCGTCCNNNNNAGATCGGAAGAGCGTCGTG/3ddC/

L17clip2.0
/5Phos/NNNNCAACTANNNNNAGATCGGAAGAGCGTCGTG/3ddC/

L18clip2.0
/5Phos/NNNNGTCCGCNNNNNAGATCGGAAGAGCGTCGTG/3ddC/

P5Solexa_s
ACACGACGCTCTTCCGATCT

P3Solexa_s
CTGAACCGCTCTTCCGATCT

P5Solexa
AATGATACGGCGACCACCGAGATCTACACTCTTTCCCTACACGACGCTCTTCC
GATCT

P3Solexa
CAAGCAGAAGACGGCATACGAGATCGGTCTCGGCATTCCTGCTGAACCGCTC
TTCCGATCT

Supplementary Figure 1: Optimisation of washing conditions for U2AF2 immunoprecipitation.

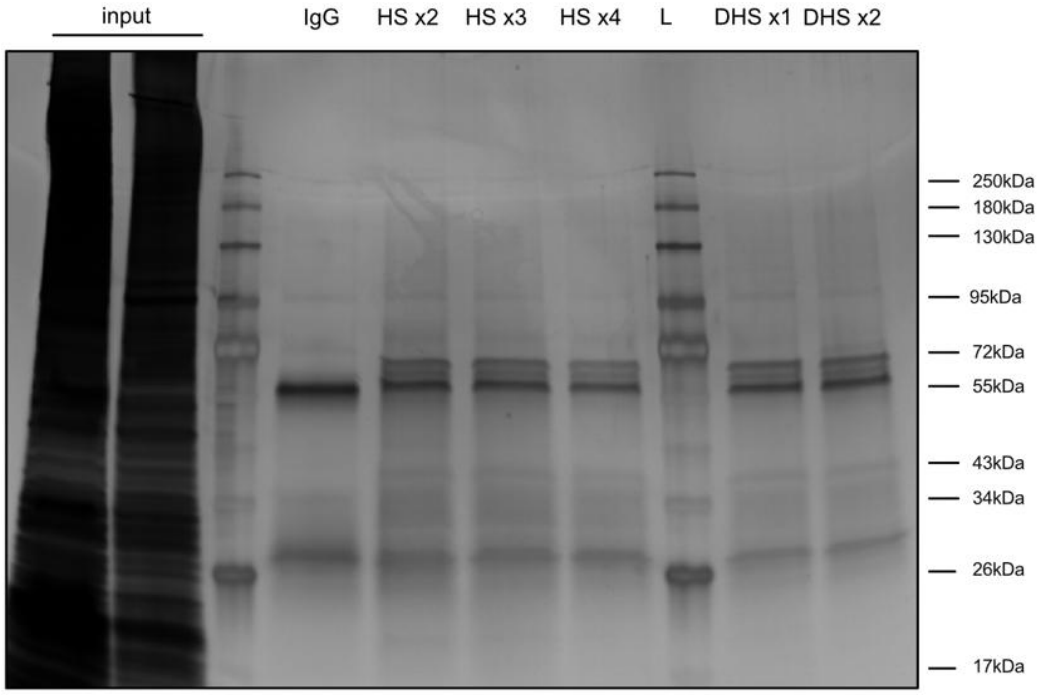

Silver staining of U2AF2 immunoprecipitation samples under different washing conditions. From left to right: whole-cell lysate input; IgG control; samples washed with high-salt buffer twice (HS ×2), three times (HS ×3), or four times (HS ×4); molecular weight ladder (L); and samples washed twice with high-salt buffer followed by one (DHS ×1) or two additional washes (DHS ×2) with doubled-salt buffer.

Supplementary Figure 2: Library size distribution assessed by TapeStation HS D5000.

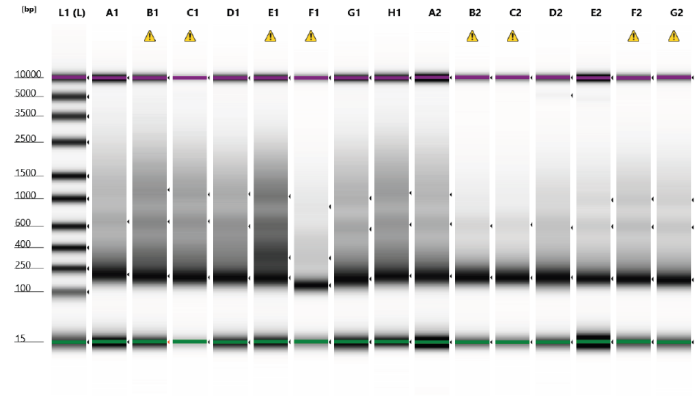

Default image (Contrast 50%), Image is Scaled to Highest Sample Peak

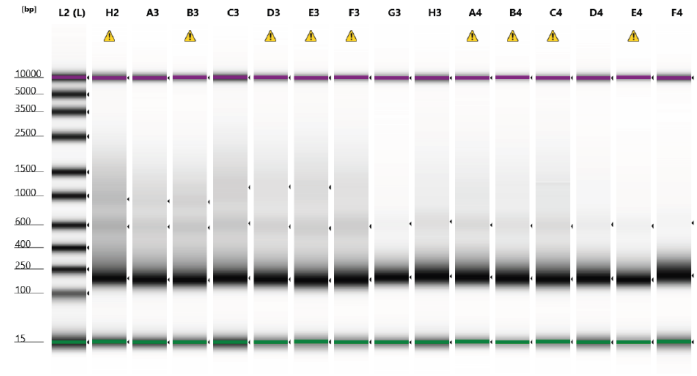

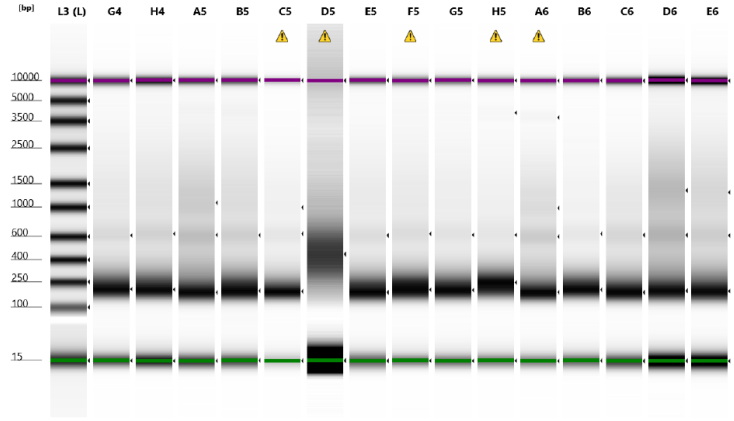

Default image (Contrast 50%), Image is Scaled to Highest Sample Peak

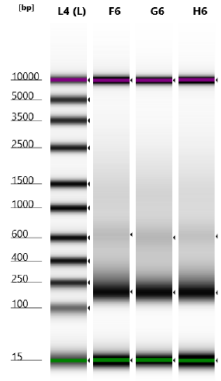

Supplementary Figure 2 (on page 50): TapeStation HS D5000 profiles showing the size distributions of iCLIP2 libraries generated from infected and mock samples following immunoprecipitation of SF3B1, AQR, SF1, and U2AF2, together with the corresponding size-matched input controls (SMI130 and SMI55).

Samples positions are as follows:

L1: Ladder, A1: R1_infected_SF3B1, B1: R2_infected_SF3B1, C1: R3_infected_SF3B1, D1: R1_mock_SF3B1, E1: R2_mock_SF3B1, F1: R3_mock_SF3B1, G1: R1_infected_AQR, H1: R2_infected_AQR, A2: R3_infected_AQR, B2: R1_mock_AQR, C2: R2_mock_AQR, D2: R3_mock_AQR, E2: R1_infected_SMI130, F2: R2_infected_SMI130, G2: R3_infected_SMI130, L2: Ladder, H2: R1_mock_SMI130, A3: R2_mock_SMI130, B3: R3_mock_SMI130, C3: R1_infected_SF1, D3: R2_infected_SF1, E3: R3_infected_SF1, F3: R1_mock_SF1, G3: R2_mock_SF1, H3: R3_mock_SF1, A4: R4_infected_SF1, B4: R5_infected_SF1, C4: R6_infected_SF1, D4: R4_mock_SF1, E4: R5_mock_SF1, F4: R6_mock_SF1, L3: Ladder, G4: R1_infected_SMI55, H4: R2_infected_SMI55, A5: R3_infected_SMI55, B5: R1_mock_SMI55, C5: R2_mock_SMI55, D5: R3_mock_SMI55, E5: R4_infected_SMI55, F5: R5_infected_SMI55, G5: R6_infected_SMI55, H5: R4_mock_SMI55, A6: R5_mock_SMI55, B6: R6_mock_SMI55, C6: R4_infected_U2AF2, D6: R5_infected_U2AF2, E6: R6_infected_U2AF2, L4: Ladder, F6: R4_mock_U2AF2, G6: R5_mock_U2AF2, H6: R6_mock_U2AF2.

Supplementary Table 1: Library size distribution and percentage distribution

Sample Description	From [bp]	To [bp]	Average Size [bp]	Conc. [pg/l]	Region Molarity [pmol/l]	% of Total
R3_mock_SMI55	100	300	226	524000	3910000	12.4
R2_mock_SF3B1	100	300	206	589	4800	26.47
R2_infected_SF3B1	100	300	208	573	4560	27.97
R2_infected_AQR	100	300	208	478	3810	29.6
R3_infected_SF3B1	100	300	205	2060	16600	31.41
R1_mock_SF3B1	100	300	203	589	4820	32.36
R1_infected_SF3B1	100	300	215	395	3030	33.43
R3_infected_AQR	100	300	206	312	2520	34.78
R5_infected_U2AF2	100	300	202	312	2540	36.14
R1_infected_AQR	100	300	196	538	4600	37.13
R1_mock_SMI130	100	300	202	683	5580	38.72
R3_infected_SMI55	100	300	199	637	5290	41.63
R4_mock_U2AF2	100	300	201	363	2990	42.44
R5_mock_U2AF2	100	300	197	401	3360	43.46
R2_infected_SMI130	100	300	194	673	5760	44.46
R1_infected_SF1	100	300	201	587	4820	44.55
R6_mock_U2AF2	100	300	200	355	2930	45.48
R6_infected_U2AF2	100	300	202	361	2960	45.82
R1_infected_SMI130	100	300	194	290	2470	46.68
R3_infected_SMI130	100	300	189	720	6330	46.81
R3_mock_AQR	100	300	198	729	6150	48.31
R3_mock_SMI130	100	300	195	896	7620	48.81
R2_infected_SMI55	100	300	210	475	3710	49.26
R2_mock_SMI130	100	300	194	693	5910	49.49
R1_mock_SMI55	100	300	203	725	5880	49.67

R3_infected_SF1	100	300	189	928	8160	49.85
R3_mock_SF3B1	100	300	163	793	8190	49.92
R5_mock_SMI55	100	300	197	906	7570	50.57
R2_infected_SF1	100	300	196	866	7310	51.96
R1_mock_SF1	100	300	193	1110	9570	52.09
R1_infected_SMI55	100	300	209	595	4650	53.58
R4_infected_U2AF2	100	300	198	600	4990	56.18
R4_infected_SF1	100	300	205	1060	8480	56.52
R3_mock_SF1	100	300	209	759	5960	56.98
R6_infected_SF1	100	300	197	1130	9500	57.15
R5_infected_SMI55	100	300	209	881	6920	57.17
R1_mock_AQR	100	300	200	832	6860	57.86
R2_mock_AQR	100	300	198	896	7440	58.48
R4_infected_SMI55	100	300	199	762	6310	59.12
R6_infected_SMI55	100	300	206	771	6130	60.04
R4_mock_SMI55	100	300	221	829	6130	60.05
R5_infected_SF1	100	300	199	1480	12200	60.99
R6_mock_SMI55	100	300	209	776	6040	64.64
R2_mock_SMI55	100	300	196	1640	13600	65.66
R4_mock_SF1	100	300	200	789	6490	68.25
R6_mock_SF1	100	300	213	732	5610	71.75
R2_mock_SF1	100	300	203	894	7150	72.93
R5_mock_SF1	100	300	190	1040	8990	75.16

Supplementary Table 1 (on page 51): Library distribution obtained from TapeStation HS D5000 analysis. For each sample in infected and mock conditions, the table reports the average fragment size (bp), concentration (pg/µL), region molarity (pmol/l), and percentage of total library.

Supplementary Figure 3: Library size distribution by TapeStation HS D5000 after reverse selection.

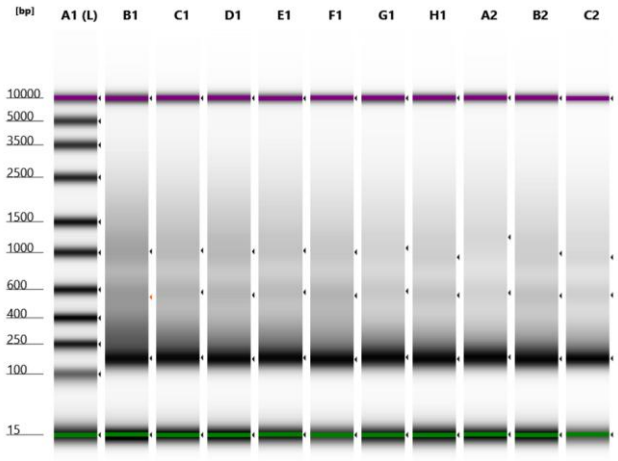

TapeStation HS D5000 profiles showing the size distributions of selected iCLIP2 libraries following reverse size selection to reduce the proportion of large DNA fragments (>300 bp). Reverse size selection was performed on libraries that contained a high proportion of fragments above the desired library size range.

Supplementary Table 2: Library size distribution and percentage distribution by TapeStation HS D5000 after reverse selection.

samples	% Large Material Before Reverse Cleanup	% Large Material After Cleanup
SF3B1_R2_MOCK	58.86	52.99
SF3B1_R2_INFECT	57.25	48.24
AQR_R2_INFECT	56.07	48.93
SF3B1_R3_INFECT	55.4	46.53
SF3B1_R1_MOCK	53.66	45.97
SF3B1_R1_INFECT	50.13	40.84
AQR_R3_INFECT	49.36	42.13
U2AF2_R5_INFECT	50.84	40.02
AQR_R1_INFECT	48.89	42.64
SMI130_R1_MOCK	47.36	39.36

Library distribution obtained from TapeStation HS D5000 analysis for the reverse-selected samples before and after the cleanup. (Average difference =8.017%)

Supplementary Figure 4: U2AF complex knockdown during RRV and SFV infection.

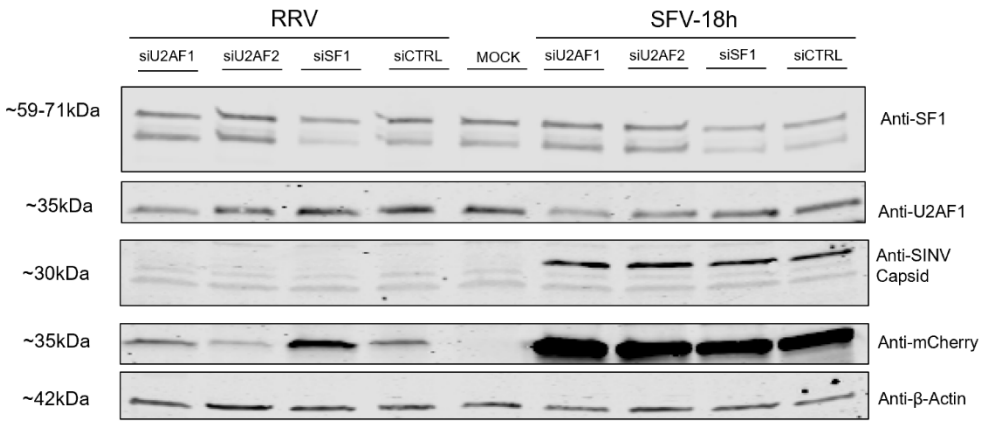

Western blot analysis of HEK293 cells transfected with siRNAs targeting U2AF1, U2AF2, or SF1, or with a non-targeting control siRNA, followed by infection with RRV-mScarlet or SFV (MOI = 0.5). These experiments were performed as exploratory optimisation trials to assess the effects of U2AF complex knockdown during RRV and SFV infection.

Supplementary Table 3: Materials

Reagent	Supplier	Identifier
10% fetal bovine serum	Gibco	10500064
streptomycin	Sigma-Aldrich	P4458
X-tremeGENE 360 transfection reagent	Roche	41106502
1× Phosphate-buffered saline	Gibco	41161501
10x Tris/Glycine/SDS Running buffer	BioRad	1610732
2X Phusion HF PCR Master mix	NEB	M0531L
4–15% Mini-PROTEAN TGX Precast protein gel	BioRad	4561084
DMEM	Gibco	11965092
DTT	Sigma Aldrich	D1532
EvaGreen	Biotium	31000
FastAP alkaline phosphatase	ThermoFisher	EF0654
ProNex	Promega	NG2001
Proteinase K	Roche	3115828001
RecJf endonuclease	New England Biolabs	M0264S
RiboLock RNase Inhibitor	ThermoFisher	EO0381
TurboDNase	ThermoFisher	AM2238
Dynabeads™ Protein A	ThermoFisher	10002D
Dynabeads™ Protein G	ThermoFisher	10009D
Ambion Rnase	ThermoFisher	AM2294
10× T4 ligation buffer	ThermoFisher	EL0021
T4 Polynucleotide Kinase	NEB	M0201L
PEG8000	MERCK	P1458
DMSO	ThermoFisher	D12345
NEB Buffer 2	NEB	B7002S
5' Deadenylase	NEB	M0331S
MyONE magnetic beads	ThermoFisher	
SuperScript IV enzyme	ThermoFisher	18090010
AEBSF	BioChemica	A14210100
Benzonase Nuclease	Millipore	E1014